IEEE Access
Multidisciplinary | Rapid Review | Open Access Journal

Received August 8, 2018, accepted September 14, 2018, date of publication September 28, 2018, date of current version October 19, 2018.

Digital Object Identifier 10.1109/ACCESS.2018.2872793

Non-Orthogonal Pilot Designs for Joint Channel Estimation and Collision Detection in Grant-Free Access Systems

AYON QUAYUM[1], (Student Member, IEEE), HLAING MINN[1], (Fellow, IEEE), AND YUICHI KAKISHIMA[2]

[1]Electrical and Computer Engineering Department, The University of Texas at Dallas, Richardson, TX 75080, USA
[2]DOCOMO Innovations Inc., Palo Alto, CA 94304, USA

Corresponding author: Ayon Quayum (ayonqm@gmail.com)

ABSTRACT In this paper, we consider a densely deployed phantom cell system providing a low latency network for massive connectivity. Non-orthogonal pilot designs serve as a promising solution to support a large number of users, but fast collision detection at the receiver is needed for low latency networks. Recently, a nice solution based on an on–off type non-orthogonal pilot design with collision detection capability has been proposed. It can serve more users than the orthogonal pilot design but at the cost of degraded channel estimation performance compared to the orthogonal optimum pilot design. We propose a new non-orthogonal pilot design with collision detection capability and improved channel estimation performance. An optimum threshold-based detection criterion is developed. We further show that a dynamically calculated optimum threshold-based detection outperforms a fixed threshold-based detection. Next, we investigate non-orthogonal pilot designs for fractional bandwidth allocation. We propose two new non-orthogonal pilot designs for physical resource block based resource allocation. Both of the new designs support fast collision detection at the receiver. Performance evaluation results show that the proposed schemes provide equivalent or better channel estimation performance and support much more users than the orthogonal pilots defined in the current 4G standards. Finally, we explore sparse channel estimation with compressed sensing technique. We prove several propositions regarding compressed sensing based estimation performance. Using these propositions, two novel orthogonal pilot designs are developed for sparse channel estimation with optimized performances. Finally, utilizing these orthogonal pilot sets, we propose a non-orthogonal pilot design with collision detection capability for sparse channel estimation.

INDEX TERMS Small cell, channel estimation, non-orthogonal pilot, pilot collision, grant-free access, compressed sensing, sparse channel.

I. INTRODUCTION

Growth of wireless traffic, densification of users and low latency requirements have created unique challenges for future wireless systems. 5G and other future standards are expected to provide support for high throughput, low latency and massive connectivity [1]. Different technologies are proposed and are being actively evaluated to achieve these goals. For example, small cell concept is used in different contexts to achieve high throughput. Dense deployment of remote radio head (RRH) is discussed in [2]. High density or ''Big'' phantom cell system provides another solution for increasing network capacity by splitting control and user (C/U) planes of the radio link [3].

User-centric ultra-dense network is discussed in [4]. In this framework, a user-centric no-cell (UCNC) system in conjunction with grant-free non-orthogonal uplink (UL) access is demonstrated in [5]. This system supports massive connectivity with low latency and overhead. For grant-free uplink access a user could use randomly chosen resources for initial transmission instead of pre-assigned resources. This eliminates the need for random access and resource grant procedure, thus reducing latency and overhead. For grant-free uplink access, it is essential for base station (BS) to obtain channel state information (CSI) and to detect any collision from initial transmission. This could be achieved by using carefully designed embedded pilot sequences.

In existing systems, orthogonal pilot sequences are re-used based on spatial separation to minimize pilot contamination [6]. This translates to poor efficiency in the spatial reuse of pilot resources. Another approach is to create a large pool of orthogonal pilot sequences and let users choose them randomly [5]. However, large overhead is needed for a sufficient number of orthogonal pilot sequences to minimize pilot collision probabilities.

One way to reduce inefficiency and large overhead is to use non-orthogonal pilot sequences with collision detection capabilities. For non-sparse channel estimation, a nice solution based on on-off type non-orthogonal pilot codes has been proposed in [7]. This scheme uses L non-zero pilot dimensions and L' null pilot dimensions to create non-orthogonal pilot sequences from a total of $(L+L')$ pilot resources. Having detected more than L non-zero pilot dimensions indicates a collision at the receiver. Further analysis shows that sectorization could increase area multiplexing gain by resolving more collision-free users per unit area [8], [9].

Compressed sensing (CS) is a powerful technique for sparse channel estimation [10]. Different compressed sensing algorithms have been proposed that take the advantage of sparsity constraints. Among them orthogonal matching pursuit (OMP) has been discussed in [11], subspace pursuit (SP) has been proposed in [12] and linear programming based the Dantzig selector has been developed in [13]. A non-orthogonal pilot design has been used with compressed sensing channel estimation in [14].

The existing non-orthogonal pilot code designs are not optimized for sparse and non-sparse channel estimation performances. As a result, they suffer from degraded channel estimation performance. Another shortcoming is the vastly different channel estimation performances for different pilot sequences which makes this design inherently unfair to different users. In this paper, by incorporating both collision detection capability and channel estimation performance in the design, we develop novel non-orthogonal pilot designs for both full and fractional bandwidth allocations in case of non-sparse channel. For sparse channel estimation, we first propose novel orthogonal pilot designs and based on them further develop non-orthogonal pilot design. The proposed designs overcome the shortcomings of the existing designs and provide substantially better channel estimation performance and fairness to users.

The remainder of the paper is organized as follows. Section II describes the system model. Section III presents the proposed non-orthogonal pilot design for non-sparse channels and its performance. Section IV develops a collision detection criterion based on an optimum threshold at receiver. Section V proposes two non-orthogonal pilot designs for non-sparse channels in case of fractional bandwidth allocation. Section VI describes several proposals related to CS based channel estimation performances. In section VII, two novel orthogonal pilot designs are proposed for sparse channel estimation. Section VIII presents the proposed non-orthogonal pilot design for sparse channel and its performance. Finally, section IX concludes the paper and provides the CS based channel estimation algorithm as an appendix.

The following notations are used throughout this paper. $\boldsymbol{A}$ is a matrix and A_i is it's i-th column. $\boldsymbol{a}$ is a vector, a is a scalar and $\{A\}$ is a set. $||\boldsymbol{a}||$ is Euclidean norm and $|a|$ represents absolute value of a. $(.)^T$ and $(.)^H$ are the transpose and the hermitian operators respectively. The notation diag$\{\boldsymbol{a}\}$ represents a square diagonal matrix with its main diagonal elements given by vector $\boldsymbol{a}$.

II. SYSTEM MODEL

We consider a "Big" phantom cell system with dense deployment of small cells. Such a system will face severe uplink pilot contamination with growing traffic. To alleviate this problem, we consider grant-free uplink access and fast user detection for our system. Time-Division Duplexing (TDD) and uplink-downlink (UL-DL) channel reciprocity is assumed. This allows non-orthogonal pilot sequences or codes in uplink to be used for acquisition of both uplink and downlink CSI. Pilot codes are designed with fast collision detection capability. Because of grant-free uplink access a user doesn't need to go through random access procedures. Instead the user can select a non-orthogonal pilot code randomly from a set of pilot codes. This allows the support for large number of users with lower overhead. Grant-free uplink access also ensures fast transmission with low latency. BS should be able to detect a collision when more than one non-orthogonal pilot codes from the same pilot codes set are received. Thus in a densely deployed small cells system, any BS within the user's transmission range can quickly establish connection to the user if no collision is detected.

We use an orthogonal frequecy division mltiplexing (OFDM) system with discrete Fourier transform (DFT) size N. For user i, let us define the frequency domain pilot vector as $\boldsymbol{c}_i$ of length N and the time domain pilot vector as $\boldsymbol{s}_i$ of length N. The channel impulse response (CIR) vector $\boldsymbol{h}_i$ consists of L sample-spaced channel taps (we assume timing errors or different propagation delays are already absorbed into the CIR). Cyclic prefix length L_{CP} $(\geq L)$ is used. Define N-point unitary DFT matrix $\boldsymbol{F} = [\boldsymbol{f}_0, \boldsymbol{f}_1, \ldots, \boldsymbol{f}_{N-1}]$ and $\boldsymbol{F}_L = [\boldsymbol{f}_0, \boldsymbol{f}_1, \ldots, \boldsymbol{f}_{L-1}]$ where $\boldsymbol{f}_k = [1, e^{-j2\pi k/N}, \ldots, e^{-j2\pi k(N-1)/N}]^T/\sqrt{N}$. The received time domain signal vector for a single OFDM symbol from M users is given by [15]

$$\boldsymbol{y} = \sum_{i=1}^{M} \boldsymbol{S}_i \boldsymbol{h}_i + \boldsymbol{n}, \tag{1}$$

where $\boldsymbol{y} = [y_0,\ y_1,\ \ldots,\ y_{N-1}]^T$, $\boldsymbol{S_i} = \sqrt{N}\boldsymbol{F}^H \boldsymbol{C_i} \boldsymbol{F}_L$, $\boldsymbol{C_i} = \mathrm{diag}\,\{\boldsymbol{c_i}\}$ and $\boldsymbol{n}$ is zero-mean complex Gaussian noise vector of length N with covariance matrix $\sigma_n^2 \boldsymbol{I}$. Here $\boldsymbol{I}$ is identity matrix.

For sparse channel scenario, we consider time domain channel $\boldsymbol{h}_i = [h_{i0}, h_{i1}, \ldots, h_{i(L-1)}]$ to be sparse with most of the entries zero. The channel power delay profile is linearly

decreasing in log scale. The ratio of the power of h_0 to h_{L-1} is 20 dB. Position of the non-zero channel taps are random and the power of the non-zero channel taps are determined according to their position. We will use compressed sensing technique to estimate sparse channel. More details of compressed sensing techniques will be discussed in section VI.

For non-sparse channel, assuming $(\boldsymbol{S}_i^H \boldsymbol{S}_i)$ is full rank, the least-square (LS) CIR estimate for user i is given by [16]

$$\hat{\boldsymbol{h}}_i = \left(\boldsymbol{S}_i^H \boldsymbol{S}_i\right)^{-1} \boldsymbol{S}_i^H \boldsymbol{y}. \tag{2}$$

For orthogonal pilot designs, optimality is achieved when

$$\begin{aligned} \boldsymbol{S}_i^H \boldsymbol{S}_i &= E_{\text{av}} \boldsymbol{I}, \quad \forall i, \\ \boldsymbol{S}_i^H \boldsymbol{S}_j &= \boldsymbol{0}, \quad \forall i \neq j \end{aligned} \tag{3}$$

where E_{av} is average OFDM symbol energy [17]. After satisfying these conditions, the mean square error (MSE) for channel estimation is given by $\sigma_n^2 \text{tr}\left(\boldsymbol{S}_i^H \boldsymbol{S}_i\right)^{-1} = L\sigma_n^2 / E_{\text{av}}$. Several optimum orthogonal pilot designs have been discussed in [17]. However, using orthogonal pilot codes is incapable of supporting a large number of users. In this paper, we will develop non-orthogonal pilot codes based on frequency division multiplexing (FDM) type orthogonal pilot sets with cyclically equi-spaced pilot tones.

We observe some shortcomings of the existing non-orthogonal pilot design [7] in the literature. First, its average channel estimation performance is substantially degraded compared to the performance achieved by the optimum orthogonal pilot design. Second, different pilot codes may have vastly unequal channel estimation performances.

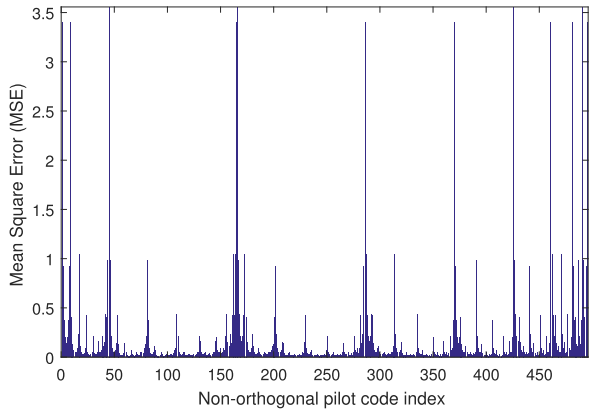

FIGURE 1. Channel estimation performance of different non-orthogonal pilot codes from the existing design (SNR=0 dB).

To illustrate these shortcomings, let us consider an example system with DFT size $N = 128$ and $L = 8$ sample-spaced channel taps. We use $L = 8$ non-zero pilot tones and $L' = 4$ null pilot tones from a total of 12 approximately evenly spaced tones. According to the existing design, null pilot tones are randomly selected from all pilot tones to create individual non-orthogonal pilot codes. There are a total of $\binom{12}{4} = 495$ non-orthogonal pilot codes possible. Fig. 1 shows channel estimation MSEs for different non-orthogonal pilot codes of the existing design for 0 dB SNR. The MSEs for different pilot codes vary substantially, which translates into unfair quality of service provisioning to different users. This also highlights the need of efficient non-orthogonal pilot designs with good channel estimation performance and capability to support a large number of users with low latency.

III. NON-ORTHOGONAL PILOTS FOR NON-SPARSE CHANNEL

A. PROPOSED PILOT DESIGN

To overcome limitations of the existing pilot design for grant-free access, we propose a novel non-orthogonal pilot design satisfying the following criteria:

- Channel estimation performance should match closely with optimum orthogonal pilot design.
- Different pilot sequences should have similar channel estimation performances to ensure fairness.
- Receiver should be able to detect collision when more than one non-orthogonal pilot codes are present.
- Pilot design should support a large number of non-orthogonal users.

The new pilot design is based on the FDM type orthogonal pilot tone index sets described in [17] for estimating L sample-spaced channel taps. In this orthogonal pilot design, each pilot set contains L cyclically equi-spaced equal energy pilot tones. Our non-orthogonal pilot design is described as follows.

1) For DFT size N, we define the total number of orthogonal sets $D = N/L$ and their pilot tone index set $\{J_k : k = 0, 1 \ldots D-1\}$ according to the FDM design in [17] where $J_k = J_{k-1} + 1$. The set J_0 which contains indexes 0 and $N/2$ (i.e., the DC tone and the band-edge tone which are typically set to be null tones), is treated separately. Define the total number of remaining pilot index sets as $D' = D - 1$.
2) Define $J_{k,a} \triangleq \{J_k[i] : i = 1, 3, 5, \ldots\}$, $k = 1, 2 \ldots D'$ and $J_{k,b} \triangleq \{J_k[i] : i = 2, 4, 6, \ldots\}$, $k = 1, 2 \ldots D'$. Also define $\tilde{D} = \left\lfloor \frac{D'}{3} \right\rfloor$. Then, each of the $2\tilde{D}$ pilot groups defined by their pilot tone index sets $\{\tilde{J}_k\}$ is constructed by combining two contiguous orthogonal pilot tone index sets in the following way:

$$\begin{aligned} \tilde{J}_1 &= J_1 \cup J_{2,a}, \quad \tilde{J}_2 = J_3 \cup J_{2,b} \\ \tilde{J}_3 &= J_4 \cup J_{5,a}, \quad \tilde{J}_4 = J_6 \cup J_{5,b} \\ &\cdots\cdots\cdots \\ \tilde{J}_{2(\tilde{D}-1)+1} &= J_{3(\tilde{D}-1)+1} \cup J_{3(\tilde{D}-1)+2,a} \\ \tilde{J}_{2(\tilde{D}-1)+2} &= J_{3(\tilde{D}-1)+3} \cup J_{3(\tilde{D}-1)+2,b} \end{aligned}$$

3) Each group's pilot tone index set $\tilde{J}_k$ contains $L/2$ pairs of pilot tones where the two tones in each pair are adjacent and $L/2$ unpaired pilot tones. Each pair is composed of one non-zero pilot tone and one null pilot tone while unpaired ones are non-zero pilots tones. All the L non-zero pilot tones within $\tilde{J}_k$ have the same amplitude a. Selecting $L/2$ non-zero pilots from $L/2$

TABLE 1. Pilot Resource Amount and the Number of Supported Users for Different Pilot Designs

BW allocation	Design	# of pilot REs per pilot group	# of orthogonal pilot groups	# of users supported per pilot group	total # of users supported
Full BW allocation	Orthogonal	8	15	1	15
	Proposed non-orthogonal	12	10	16	160
Fractional BW allocation	Orthogonal (4G standards)	16	1	1	1
	Proposed non-orthogonal Scheme A ($r = 2$)	20	1	16	16
	Proposed non-orthogonal Scheme B	16	1	128	128

pairs yields $2^{L/2}$ non-orthogonal pilot codes within the pilot group defined by $\tilde{J}_k$.

4) Non-zero tones from J_0 and $\left\{J_k : k = 3\tilde{D} + 1 \ldots D'\right\}$ can be distributed to adjacent $\tilde{J}_k$ sets as evenly as possible. For example, define $(L-2)$ non-zero tones of J_0 as $J_0' = \left\{J_0 \backslash \left\{0, \frac{N}{2}\right\}\right\}$. Then, we can add $J_{0,a}'$ to $\tilde{J}_1$ and $J_{0,b}'$ to $\tilde{J}_{\tilde{D}}$. In this case, the pilot groups defined by $\tilde{J}_1$ and $\tilde{J}_{\tilde{D}}$ have 2^{L-1} non-orthogonal pilot codes in each group.

Channel estimation MSE of the proposed pilot code k from the group based on $\tilde{J}_i$, if without collision within the group, is given by $\sigma_n^2 \mathrm{tr}(\boldsymbol{S}_k^H \boldsymbol{S}_k)^{-1}$. Due to the choice of adjacent tones for pilot pairs, some pilot codes will maintain $\boldsymbol{S}_k^H \boldsymbol{S}_k = E_{\mathrm{av}} \boldsymbol{I}$ while the others will have $\boldsymbol{S}_k^H \boldsymbol{S}_k \approx E_{\mathrm{av}} \boldsymbol{I}$. Note that phases of the non-zero pilot sequence do not affect MSE and hence they can be designed to yield low peak to average power ratio (PAPR) of the time domain signal.

To illustrate our non-orthogonal pilot design, let us consider a system with DFT size of $N = 128$ and $L = 8$ sample-spaced channel taps. Each FDM orthogonal pilot set consists of $L = 8$ pilot tones. If we exclude J_0 due to practical setting of null tones at index 0 and $N/2$, the total number of orthogonal pilot sets is $D = 15$. The proposed non-orthogonal pilot tone index sets are:

$$\tilde{J}_1 = [(1\ 2)\ 17\ (33\ 34)\ 49\ (65\ 66)\ 81\ (97\ 98)\ 113]$$

$$\tilde{J}_2 = [3\ (18\ 19)\ 35\ (50\ 51)\ 67\ (82\ 83)\ 99\ (114\ 115)]$$

$$\ldots\ldots\ldots$$

$$\tilde{J}_{10} = [15\ (30\ 31)\ 47\ (62\ 63)\ 79\ (94\ 95)\ 111\ (126\ 127)]$$

where the indexes of pilot pairs are shown in the bracket. There are 10 orthogonal pilot groups defined by $\{\tilde{J}_1, \ldots, \tilde{J}_{10}\}$ and each group has $2^4 = 16$ non-orthogonal pilot codes since there are 4 pairs of adjacent pilot tones. Each pilot code has 4 null pilot tones (one from each pilot tone pair) and 8 non-zero pilot tones with amplitude a on the remaining tones. For example, within the group $\tilde{J}_1$, the non-zero pilot tone indexes of the first four non-orthogonal pilot codes are {1, 33, 65, 97, 17, 49, 81, 113}, {2, 33, 65, 97, 17, 49, 81, 113}, {1, 34, 65, 97, 17, 49, 81, 113}, and {2, 34, 65, 97, 17, 49, 81, 113}. Fig. 2 shows an example of designing non-orthogonal pilot groups from orthogonal pilot sets. Table 1 provides details about the pilot resource amount and the number of users supported by different pilot designs.

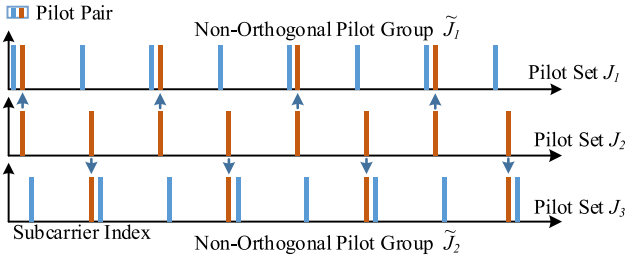

FIGURE 2. Design of non-orthogonal pilot codes from orthogonal pilot sets.

In existing orthogonal pilot design, there are several orthogonal pilot sets where each set can support only one pilot code. Our new pilot design has smaller number of orthogonal pilot sets while each set can support multiple pilot codes. Different orthogonal pilot sets could be used for different antennas or different user groups. So the new pilot design is easily applicable for multiple antenna systems.

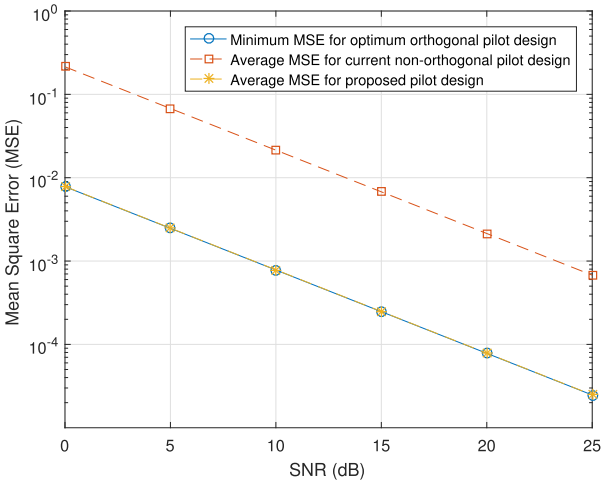

FIGURE 3. Channel estimation performance comparison among different pilot designs in a system with $N = 128$ subcarriers and $L = 8$ channel taps.

B. CHANNEL ESTIMATION PERFORMANCE

Fig. 3 compares channel estimation performance of the proposed non-orthogonal pilot codes with that of orthogonal optimum design and the existing non-orthogonal design.

The proposed design provides an improvement of around 15 dB compared to the existing non-orthogonal design and its performance closely matches that of orthogonal design.

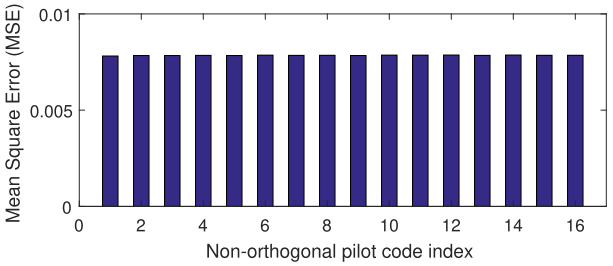

FIGURE 4. Channel estimation performance of the proposed non-orthogonal pilot codes within a pilot group (SNR=0 dB).

Fig. 4 shows the channel estimation MSE for different non-orthogonal pilot codes within a pilot group of the proposed design. By comparing the corresponding results of the existing design in Fig. 1, we can observe that the MSE performances for different codes are essentially the same for the proposed design while they vary substantially for the existing design. Thus, the proposed non-orthogonal pilot design offers fairness to different users.

IV. THRESHOLD-BASED PILOT DETECTION

At the receiver, the energy of each pilot tone in a pilot index set $\tilde{J}_k$ is compared with a predefined detection threshold. The receiver detects a non-zero pilot tone if the received energy on that tone exceeds the detection threshold. A single user is detected if exactly L non-zero pilot tones are detected and the non-zero tones correspond to a valid pilot index set $\tilde{J}_k$. A collision is detected if more than L non-zero pilot tones are detected. Otherwise, no user is detected. Next, we will consider the threshold-based pilot detection performance. We will define two performance metrics: probability of single user detection (P_{SUD}) and probability of collision detection (P_{CD}). P_{SUD} is defined as the probability of detecting the pilot correctly when only one user transmits the pilot code and P_{CD} is defined as the probability of detecting a collision when more than one user transmit non-orthogonal pilot codes within a pilot codes group.

A. PROBABILITY OF SINGLE USER DETECTION (P_{SUD})

Non-zero pilot tones are detected based on the received energy levels of the pilot subcarriers. For the threshold based detection, the energy of each of the possible pilot tones in a pilot codes set is compared to a predefined threshold value to determine an active or null pilot. Let us consider the received energies of a pilot code consisting of L active pilot tones of indexes $(q_1, q_2 \dots q_L)$ and L' null tones of indexes $(q'_1, q'_2 \dots q'_{L'})$. Also define the ratio (L'/L) as γ, the transmit pilot power on each non-zero pilot tone as a^2 and noise power per tone as N_0. Frequency domain received signal is $\boldsymbol{Y} = \boldsymbol{F}\boldsymbol{y}$ where $\boldsymbol{Y} = [Y_0\ Y_1\ \dots\ Y_{N-1}]^T$. For a Rayleigh fading channel, the average received power on a pilot subcarrier is given by

$$E\left[|Y_k|^2\right] = \begin{cases} a^2 + N_0, & k \in q \\ N_0, & k \in q' \end{cases} \tag{4}$$

The SNR is defined as $\text{SNR} = \frac{E_{\text{av}}}{NN_0}$ where $E_{\text{av}} = La^2$.

Let the detection threshold be τ. Then, P_{SUD} is given by

$$P_{\text{SUD}} = P\big[\big(\cap_{i\in\{q_l\}}\left(|Y_i|^2 > \tau\right)\big) \cap \big(\cap_{j\in\{q'_l\}}\left(|Y_j|^2 < \tau\right)\big)\big]$$

Assuming all received pilot tones are independent, we can compute the probability of single user detection as

$$\begin{aligned} P_{\text{SUD}} &= \Big[\prod_{i\in\{q_l\}} P\left(|Y_i|^2 > \tau\right)\Big]\Big[\prod_{j\in\{q'_l\}} P\left(|Y_j|^2 < \tau\right)\Big] \\ &= \big[1 - F\big(\frac{2\tau}{a^2+N_0}\big)\big]^L\big[F\big(\frac{2\tau}{N_0}\big)\big]^{L'} \end{aligned} \tag{5}$$

where $F(x)$ is an exponential cumulative distribution function given by

$$F(x) = 1 - e^{-\frac{x}{2}}. \tag{6}$$

Substituting (6) in (5) and using $L' = \gamma L$, we get

$$P_{\text{SUD}} = \big[e^{-\left(\frac{2\tau}{2(a^2+N_0)}\right)}\big]^L\big[1 - e^{-\left(\frac{2\tau}{2N_0}\right)}\big]^{\gamma L}. \tag{7}$$

Now, we can find the optimum detection threshold by maximizing P_{SUD} as follows. First, we take the first derivative of P_{SUD} and equate it to zero as

$$\frac{d}{d\tau}\Big(\big[e^{-\left(\frac{\tau}{(a^2+N_0)}\right)}\big]^L\big[1 - e^{-\left(\frac{\tau}{N_0}\right)}\big]^{\gamma L}\Big) = 0. \tag{8}$$

By solving (8), we obtain the optimum detection threshold as

$$\tau_{\text{opt}} = -N_0 \ln\Big(\frac{L}{\gamma N\ \text{SNR} + L(1+\gamma)}\Big). \tag{9}$$

Equation (9) shows that the optimum value of the detection threshold depends on the SNR value. The threshold can be set based on the targeted SNR of the considered application, which we call a fixed threshold setting.

Alternatively, we can calculate τ_{opt} based on the instantaneous SNR estimate and use it as a detection threshold. This dynamic threshold setting improves the detection performance compared to the fixed threshold setting. To illustrate the performance gain from the dynamic detection threshold, we consider the previous example with DFT size 128 and 8 non-zero pilot tones per pilot group. Fig. 5 shows P_{SUD} using a fixed threshold ($\tau = 1$) and a dynamic threshold for different SNRs. The fixed threshold is only optimum for a certain SNR value. In all other cases, the dynamic threshold provides performance gain.

B. PROBABILITY OF COLLISION DETECTION (P_{CD})

Another important performance metric is the probability of collision detection P_{CD}. We use the previous example to illustrate the effect of the detection threshold for P_{CD}. We use scenarios with two non-orthogonal pilot users within a pilot group in Fig. 6(a) and three users within a pilot

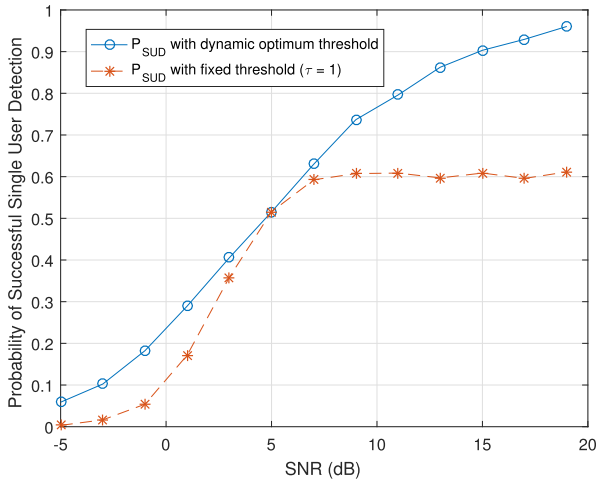

FIGURE 5. Single user detection performance for the dynamic versus fixed detection threshold settings.

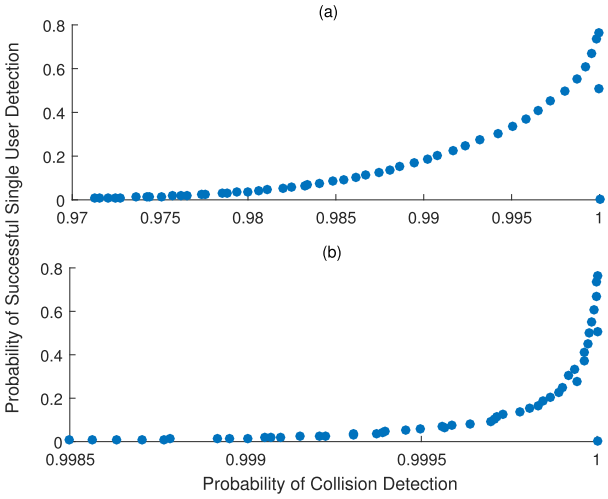

FIGURE 6. Single user detection performance versus collision detection performance for different detection threshold values. a) 2 users per pilot group, b) 3 users per pilot group.

group in Fig. 6(b). In our simulation, all users have the same SNR. We plot P_{SUD} against P_{CD} for 10 dB SNR. In the plot each point corresponds to a different detection threshold value. Fig. 6 shows that the optimum threshold for P_{SUD} also provides high probability of collision detection. So we can conclude that the optimum detection threshold for the single user detection performance is also a good choice for the collision detection performance.

V. DESIGN FOR FRACTIONAL BANDWIDTH ALLOCATION

Now we will develop two different pilot schemes for fractional bandwidth (BW) allocation, denoted as Scheme A and B. Both of them use Physical Resource Block (PRB) similar to what is defined in 4G standards for 3GPP Long Term Evolution (LTE) downlink reference signal (RS) as a resource allocation unit. Each PRB consists of 12 subcarriers and 7 symbols (1 time slot). A single symbol and one subcarrier creates time-frequency resource element (RE). We consider few REs to be dedicated for pilot sequences in each PRB. Other REs will be used for data transmission. For both of the schemes, we will use the concept of pilot pairs similar to our non-orthogonal pilot design in Section III.

A. SCHEME A

In LTE standards, two pilot tones are used in each of first and third from the last OFDM symbol of each time slot. The two pilot tones in one OFDM symbol is evenly distributed in a PRB with 6 subcarriers spacing between them. We propose one additional pilot tone in the first OFDM symbol of every r-th PRB. The additional pilot RE will be placed adjacent to one of the existing pilot subcarriers. These two adjacent pilot tones will create a pilot pair. To create non-orthogonal pilot codes, we will use one non-zero pilot and one null pilot from each pilot pair allocated in a pilot set. If the number of PRBs allocated with additional pilots is S, the pilot set can have up to 2^S non-orthogonal pilot codes.

B. SCHEME B

Scheme B is suitable when the allocated PRBs are contiguous in frequency. We use two pilot tones in each of first and third from the last OFDM symbol of each time slot. We use first and last subcarrier in each of these OFDM symbols as pilot tones. First subcarrier of the first allocated PRB and last subcarrier of the last allocated PRB are always used as non-zero pilots. For the remaining PRBs, last and first pilots of adjacent PRBs will create a pilot pair which are contiguous in frequency. We use one non-zero pilot from each available pilot pair to create non-orthogonal pilot codes. A pilot set has $(T+1)$ non zero pilots and can support up to $2^{(T-1)}$ non-orthogonal pilot codes where T is the total number of allocated PRBs.

Fig. 7 shows pilot locations for Scheme A and Scheme B where adjacent pilot tones are used as pilot pairs.

Table 1 summarizes the numbers of users supported and pilot resources used by different pilot designs.

C. CHANNEL ESTIMATION PERFORMANCE FOR FRACTIONAL BANDWIDTH

To evaluate channel estimation performance for these schemes, let us assume R consecutive tones at indexes $(r_1, r_2 \ldots r_R)$ are allocated to each user. We consider the channel to be time-invariant for the span of one PRB. Thus, we will use just one OFDM symbol for channel estimation. Let $\boldsymbol{X_P} = \text{diag}\{c_{q_1}, c_{q_2} \ldots c_{q_P}\}$ be a diagonal matrix with non-zero pilot tones as its diagonal elements and $\boldsymbol{H}_P = [H_{q_1} H_{q_2} \ldots H_{q_P}]^T$ be the channel frequency response (CFR) of the pilot subcarriers. Then the received frequency domain pilot vector for the considered pilot code is given by

$$\boldsymbol{Y}_P = \boldsymbol{X}_P \boldsymbol{H}_P + \boldsymbol{N}_P \tag{10}$$

where $\boldsymbol{N}_P$ is the noise vector on pilot subcarriers with covariance $\sigma_n^2 \boldsymbol{I}$. For L sample-spaced channel taps, the estimate of

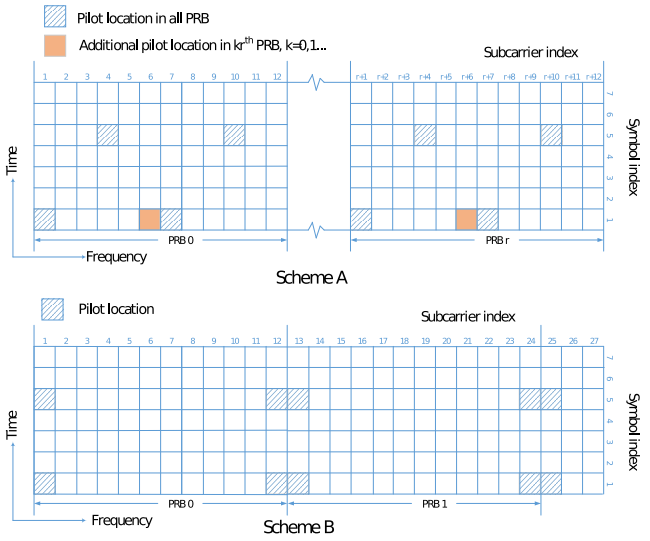

FIGURE 7. Proposed pilot Scheme A and Scheme B for the fractional bandwidth allocation.

CFR for allocated bandwidth of R tones is given by

$$\hat{\boldsymbol{H}}_R = \boldsymbol{F}_R \left(\boldsymbol{F}_{PL}^H \boldsymbol{F}_{PL}\right)^{-1} \boldsymbol{F}_{PL}^H \hat{\boldsymbol{H}}_P \tag{11}$$

where

$\hat{\boldsymbol{H}}_R$ = Estimate of CFR for R tones
$\hat{\boldsymbol{H}}_P = \boldsymbol{X}_P^{-1}\boldsymbol{Y}_P$, LS estimate of CFR for P pilot tones
$\boldsymbol{F}_R$ = First L columns and R rows corresponding to tone indexes $(r_1, \ldots, r_R)$ of DFT matrix $\boldsymbol{F}$
$\boldsymbol{F}_{PL}$ = First L columns and P rows corresponding to pilot tone indexes $(q_1, \ldots, q_P)$ of DFT matrix $\boldsymbol{F}$

The corresponding MSE is given by

$$E\left[||\hat{\boldsymbol{H}}_R - \boldsymbol{H}_R||^2\right] = \sigma_n^2 \, \mathrm{tr}\left(\boldsymbol{A}\left(\boldsymbol{X}_P^H \boldsymbol{X}_P\right)^{-1} \boldsymbol{A}^H\right) \tag{12}$$

where $\boldsymbol{A} = \boldsymbol{F}_R\left(\boldsymbol{F}_{PL}^H \boldsymbol{F}_{PL}\right)^{-1} \boldsymbol{F}_{PL}^H$.

To compare the performance of different schemes, let us consider an example of 8 consecutive PRB allocation per user. We will use DFT size of 512 and 8 sample-spaced channel taps. Original orthogonal pilot scheme has a total of 16 non-zero pilots within the allocated bandwidth. For scheme A we will use $r = 2$ (i.e., add a new pilot RE in every other PRBs). This makes a total of 20 pilot REs and 16 non-zero pilot REs available to each user. Scheme B uses a total of 16 pilot REs and 9 non-zero pilot REs for each pilot set. Scheme A can support 16 users and Scheme B can support up to 128 users with non-orthogonal pilot codes while the original scheme can support only one user. See Table 1 for comparison. Fig. 8 shows the channel estimation performance of different pilot designs for the fractional bandwidth allocation. Scheme A and the orthogonal allocation scheme has comparable performance. Scheme B performs better compared to other schemes as its use of both band edge subcarriers for non-zero pilots yields better channel interpolation.

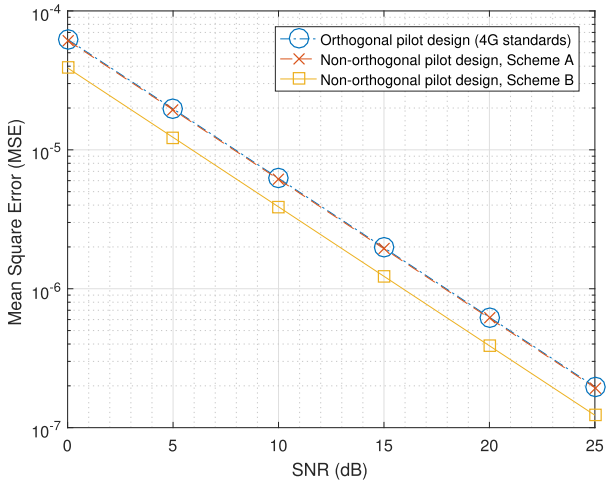

FIGURE 8. Channel estimation performance for different pilot designs in the fractional bandwidth allocation.

VI. PILOTS FOR SPARSE CHANNELS

A. PROPOSED PILOT DESIGNS

For sparse channel estimation, CS techniques can lower the number of pilot resources necessary per user. As discussed in section III, our pilot design for non-sparse channel requires the same number of non-zero pilot tones as the total number of channel taps. For CS the number of non-zero pilot tones are always lower than the total number of channel taps. We will use orthogonal matching pursuit (OMP) algorithm [11] to evaluate the channel estimation performance of different pilot codes. We choose OMP algorithm due to its low complexity and ease of implementation. The algorithm is described in the Appendix.

Proposed non-orthogonal pilot design in section III uses optimum orthogonal pilot sets as the baseline for LS based CIR estimation. But there are no equivalent techniques available in the literature to develop similar optimum orthogonal pilot sets for multi-user CS based channel estimation. So we first design orthogonal pilot sets for CS techniques. Then, we utilize the proposed orthogonal pilot sets as the basis for developing non-orthogonal pilot sequences.

Here we first describe some propositions related to the CS based channel estimation performance. Later we will use these propositions to develop orthogonal and non-orthogonal pilot sets.

Let $\{\boldsymbol{q}\} = [q_0, q_1, \ldots, q_{P-1}]$ be the P pilot tone indexes of pilot set $\boldsymbol{q}$, sorted in an increasing order, with frequency domain pilot symbols $\left[c_{q_0}, c_{q_1}, \ldots, c_{q_{P-1}}\right]$. We define sample spaced channel length $L(L > P)$ for the time domain channel $\boldsymbol{h}$ according to the discussion in section II. With zero-mean complex Gaussian noise vector $\boldsymbol{n}$, the received frequency domain pilot vector for the considered pilot code is given by

$$\boldsymbol{Y_P} = \sqrt{N}\boldsymbol{C}\boldsymbol{F}_{\mathrm{PL}}\boldsymbol{h} + \boldsymbol{n} \tag{13}$$

where

$\boldsymbol{Y_P} = [Y_0, Y_2, \ldots, Y_{P-1}]^T$
$\boldsymbol{C} = \mathrm{diag}\left\{c_{q_0}, c_{q_1}, \ldots, c_{q_{(P-1)}}\right\}$

$$\boldsymbol{h} = [h_0, h_1, \ldots, h_{L-1}]^T$$
$$\boldsymbol{n} = \left[n_0, n_1, \ldots, n_{(P-1)}\right]^T$$
$$\boldsymbol{F}_{\mathrm{PL}} = P \text{ rows corresponding to the pilot tone indexes and first } L \text{ columns of the DFT matrix } \boldsymbol{F}.$$

Definition 1: For the pilot tones index set $\boldsymbol{q}$, define *dictionary matrix*, $\boldsymbol{A}(\boldsymbol{q}) = \sqrt{N}\boldsymbol{C}\boldsymbol{F}_{\mathrm{PL}}$. Properties of the dictionary matrix determines the channel estimation performance in compressed sensing system. The received frequency domain pilot vector is given by

$$\boldsymbol{Y_P} = \boldsymbol{A}(\boldsymbol{q})\boldsymbol{h} + \boldsymbol{n} \tag{14}$$

Definition 2: For the pilot tones index set $\boldsymbol{q}$, the *coherence* $g(\boldsymbol{q})$ is defined as the maximum absolute correlation between two columns of the dictionary matrix $\boldsymbol{A}(\boldsymbol{q})$,

$$g\left(\boldsymbol{q}\right) = \max_{0 \le m < n \le L-1} |\langle A_m, A_n \rangle|, \tag{15}$$

where A_i is the ith column of the dictionary matrix $\boldsymbol{A}(\boldsymbol{q})$. Let us define $d = n - m$. Then the coherence is given by

$$g\left(\boldsymbol{q}\right) = \max_{1 \le d \le L-1} \left| \sum_{k=0}^{P-1} \left|c_{q_k}\right|^2 e^{-j\frac{2\pi}{N} q_k d} \right|. \tag{16}$$

Coherence is closely related to channel estimation performance [18], [19]. Lower coherence indicates a better performance.

We will use different properties of the dictionary matrix and coherence to develop new pilot designs for CS based channel estimation. Here we describe several propositions that will be used later for pilot designs.

Proposition 1: Coherence is upper bounded by

$$g\left(\boldsymbol{q}\right) \le \sum_{k=0}^{P-1} \left|c_{q_k}\right|^2. \tag{17}$$

Proof: With the use of triangle inequality, we have

$$g\left(\boldsymbol{q}\right) \le \max_{1 \le d \le L-1} \sum_{k=0}^{P-1} \left| \left|c_{q_k}\right|^2 e^{-j\frac{2\pi}{N} q_k d} \right|. \tag{18}$$

Now using the fact that $\left| \left|c_{q_k}\right|^2 e^{-j\frac{2\pi}{N} q_k d} \right| = \left|c_{q_k}\right|^2$ is not dependent on d, we conclude $g\left(\boldsymbol{q}\right) \le \sum_{k=0}^{P-1} \left|c_{q_k}\right|^2$. □

Proposition 2: Coherence is maximum when all the pilot tones are cyclically equi-spaced and the total number of pilot tones P is less than the channel length L.

Proof: Let $\left\{\boldsymbol{q}'\right\} = [q'_0, q'_1 \ldots q'_{P-1}]$ be the index set of cyclically equi-spaced P pilot tones where $P < L$. The pilot tone indexes are given by

$$q'_k = \left(\frac{N}{P}k + \alpha\right);\ k \in [0, 1, \ldots, (P-1)],$$
$$\alpha \in [0, 1, \ldots, (N/P - 1)]. \tag{19}$$

By using (19) in (16), the coherence for cyclically equi-spaced pilot tones is

$$g\left(\boldsymbol{q}\right) = \max_{1 \le d \le L-1} \left| \sum_{k=0}^{P-1} \left|c_{q'_k}\right|^2 e^{-j\frac{2\pi}{N}\left(\frac{N}{P}k + \alpha\right)d} \right|. \tag{20}$$

The maximum value for the function will occur when $d = P$ and the coherence is

$$g\left(\boldsymbol{q}\right) = \left| \sum_{k=0}^{P-1} \left|c_{q'_k}\right|^2 e^{-j2\pi\left(k + \frac{\alpha P}{N}\right)} \right| = \sum_{k=0}^{P-1} \left|c_{q'_k}\right|^2. \tag{21}$$

From proposition 1, this is the maximum coherence for pilot tones with index set $\left\{\boldsymbol{q}'\right\}$. □

Proposition 3: If there exists two adjacent pilot tones that are separated by N/L or less number of subcarriers, coherence will be less than the upper bound in proposition 1, given the total number of pilot tones P is less than the channel length L.

Proof: We start by observing the fact that to achieve upper bound in proposition 1,

$$\max_d \left[\left| \left|c_{q_k}\right|^2 e^{-j\frac{2\pi}{N} q_k d} + \left|c_{q_l}\right|^2 e^{-j\frac{2\pi}{N} q_l d} \right| \right] = \left|c_{q_k}\right|^2 + \left|c_{q_l}\right|^2,$$
$$d \in [1, 2 \ldots L-1];\ k, l \in [0, 1, \ldots P-1];\quad k \ne l. \tag{22}$$

Now let $q_l = q_k + x; x \ne 0$. After substituting q_l in equation (22) and simplifying,

$$\max_d \left[\left| \left|c_{q_k}\right|^2 + \left|c_{q_l}\right|^2 e^{-j\frac{2\pi}{N} x d} \right| \right] = \left|c_{q_k}\right|^2 + \left|c_{q_l}\right|^2. \tag{23}$$

This condition is fulfilled when

$$\max_d \left(e^{-j\frac{2\pi}{N} x d} \right) = e^{-j2\pi v} = 1, \quad v \in [1, 2 \ldots]. \tag{24}$$

Let $d_m = \arg\max_d \left(e^{-j\frac{2\pi}{N} x d} \right)$. From equation (24), we can express x in terms of d_m, v and N as, $x = \frac{Nv}{d_m}$. Now using the fact that $v \ge 1$ and $d_m < L$, we find the condition, $x > \frac{N}{L}$ must be true to achieve the upper bound in proposition 1. So we conclude that if there exists any two pilot tones with distance $x \le \frac{N}{L}$, the coherence is less than the upper bound in proposition 1. □

Proposition 4: For equal energy pilot tones, coherence is not affected by the constant cyclical shift of the pilot tones. Coherence $g(\boldsymbol{q}) = g(\boldsymbol{q}_b)$ where $\{\boldsymbol{q}_b\} = [q_{b_0}, q_{b_1} \ldots q_{b_{(P-1)}}]$ and $q_{b_i} = (q_i + b) \mod N$ for an integer b.

Proof: From the definition of coherence,

$$g\left(\boldsymbol{q}_b\right) = \max_{1 \le d \le L-1} \left| \sum_{k=0}^{P-1} \left|c_{(q_{b_k})}\right|^2 e^{-j\frac{2\pi}{N}(q_{b_k})d} \right|. \tag{25}$$

For equal energy pilots, let $\left|c_{q_0}\right|^2 = \left|c_{q_1}\right|^2 = \ldots = E_p$. Now using the fact that $e^{-j\frac{2\pi d}{N}((q_k+b) \bmod N)} = e^{-j\frac{2\pi d}{N}(q_k+b)}$, the coherence is

$$g\left(\boldsymbol{q}_b\right) = E_p \max_{1 \le d \le L-1} \left| e^{-j\frac{2\pi}{N} b d} \right| \left| \sum_{k=0}^{P-1} e^{-j\frac{2\pi}{N} q_k d} \right|$$
$$= E_p \max_{1 \le d \le L-1} \left| \sum_{k=0}^{P-1} e^{-j\frac{2\pi}{N} q_k d} \right| = g\left(\boldsymbol{q}\right). \tag{26}$$

□

Proposition 5: For a pilot tones index set $\{\boldsymbol{q}\} = [q_0, q_1, \ldots, q_{P-1}]$, *define* $\{\boldsymbol{q}_R\} \triangleq \{N-\boldsymbol{q}\} = [(N-q_0), \ldots, (N-q_{P-1})]$. *Then for equal energy pilot tones, coherence* $g(\boldsymbol{q}) = g(\boldsymbol{q}_R) = g(\boldsymbol{q}_R + b)$ *for an integer* b.

Proof: For equal energy pilot tones with energy E_p, the coherence

$$g\,(N-\boldsymbol{q}) = E_p \max_{1\le d\le L-1}\left|\sum_{k=0}^{P-1} e^{-j\frac{2\pi}{N}(N-q_k)d}\right| = E_p \max_{1\le d\le L-1}\left|e^{-j2\pi d}\right|\left|\sum_{k=0}^{P-1} e^{j\frac{2\pi}{N}q_k d}\right| = g\,(\boldsymbol{q}). \tag{27}$$

Also we note that using proposition 4 for any integer b,

$$g\left(\boldsymbol{q}_R + b\right) = g\,(N-\boldsymbol{q}+b) = g\,(N-\boldsymbol{q}) = g\,(\boldsymbol{q}). \tag{28}$$

In further discussion we will use the term *mirror indexed pilot set* (MIPS) of $\{\boldsymbol{q}\}$ to specify pilot index set $\{\boldsymbol{q}_R\}$ or $\{\boldsymbol{q}_R + b\}$ with the above property. □

Definition 3: Let $\{\boldsymbol{u}_M\} = [u_0, u_1, \ldots, u_{M-1}]$ of cardinality M be a subset of $\{z_N\} = [0, 1, 2, \ldots, N-1]$ of cardinality N. Then we define *Groupwise Cyclic Difference Set* (GCDS) as a subset $\{\boldsymbol{a}(\boldsymbol{u}_M, N, K, \Lambda)\} = [a_0 \ldots a_{K-1}]$ of $\{\boldsymbol{u}_M\}$ where the cyclic differences within the members of $\{\boldsymbol{a}\}$ take each one of all the possible nonzero values of the members of $\{\boldsymbol{u}_M\}$ exactly Λ times. There are a total of $K(K-1)$ cyclic differences within the members of $\{\boldsymbol{a}\}$ given by

$$(a_i - a_j) \mod N, \quad i \ne j. \tag{29}$$

In special case when $\{\boldsymbol{u}_M\} = \{z_N\}$, the subset $\{\boldsymbol{a}(N, K, \Lambda)\}$ is commonly defined in literature as *Cyclic Difference Set* (CDS).

Proposition 6: For a channel length $L \le N$, *coherence of a pilot index set* $\{\boldsymbol{q}_a\}$ *of* P *pilot tones achieves Welch lower bound when the set* $\{\boldsymbol{q}_a(\boldsymbol{u}, N, P, \Lambda)\}$ *is GCDS with* $\left\{\boldsymbol{u} : u_m = \frac{N}{L}m; m = 0, 1, 2 \ldots (L-1)\right\}$ *and* $\Lambda = \frac{P(P-1)}{L-1}$.

Proof: From the definition of coherence,

$$g\,(\boldsymbol{q}) = E_p \max_{1\le d\le L-1}\left|\sum_{k=0}^{P-1} e^{-j\frac{2\pi}{N}q_k d}\right|. \tag{30}$$

According to Welch lower bound [20], [21] for maximum of inner products among a set of unit norm vectors,

$$\max_{1\le d\le L-1}\frac{1}{P}\left|\sum_{k=0}^{P-1} e^{-j\frac{2\pi}{N}q_k d}\right| \ge \sqrt{\frac{L-P}{(L-1)\,P}} \tag{31}$$

with equality if and only if $\forall d \in [1, \ldots, L-1]$,

$$\frac{1}{P}\left|\sum_{k=0}^{P-1} e^{-j\frac{2\pi}{N}q_k d}\right| = \sqrt{\frac{L-P}{(L-1)\,P}}. \tag{32}$$

By using Welch lower bound, the coherence is bounded by

$$g(\boldsymbol{q}) \ge E_p\sqrt{\frac{P\,(L-P)}{L-1}} \tag{33}$$

Now we define $\psi_{\boldsymbol{q}}(d),\ d \in [1, \ldots, L-1]$, as

$$\psi_{\boldsymbol{q}}(d) = \frac{1}{P^2}\left|\sum_{k=0}^{P-1} e^{-j\frac{2\pi}{N}q_k d}\right|^2 = \frac{1}{P^2}\sum_{k=0}^{P-1}\sum_{l=0}^{P-1} e^{-j\frac{2\pi}{N}(q_k-q_l)d} = \frac{1}{P^2}\left(P + \sum_{k=0}^{P-1}\sum_{l=0,l\ne k}^{P-1} e^{-j\frac{2\pi}{N}(q_k-q_l)d}\right). \tag{34}$$

Let cyclic difference among pilot tone indexes be denoted by $v = ((q_k - q_l) \mod N)$, and n_v be the number of times v appears in the last term of equation (34). Then $\psi_{\boldsymbol{q}}(d)$ could be written in terms of v and n_v as

$$\psi_{\boldsymbol{q}}(d) = \frac{1}{P} + \frac{1}{P^2}\sum_{v=1}^{N-1} n_v e^{-j\frac{2\pi}{N}vd} = \frac{L-P}{(L-1)P} + \frac{P-1}{(L-1)P} + \frac{1}{P^2}\sum_{v=1}^{N-1} n_v e^{-j\frac{2\pi}{N}vd}. \tag{35}$$

We define function $\lambda_{\boldsymbol{q}}(d)$ for $d \in [1, \ldots, L-1]$ as

$$\lambda_{\boldsymbol{q}}(d) = P^2\left(\psi_{\boldsymbol{q}}(d) - \frac{L-P}{(L-1)P}\right) = \frac{P(P-1)}{L-1} + \sum_{v=1}^{N-1} n_v e^{-j\frac{2\pi}{N}vd}. \tag{36}$$

By defining $n_0 = \frac{P(P-1)}{L-1}$, $\{\lambda_{\boldsymbol{q}}(d)\}$ and $\{n_v\}$ form a DFT pair where

$$\lambda_{\boldsymbol{q}}(d) = \sum_{v=0}^{N-1} n_v e^{-j\frac{2\pi}{N}vd}. \tag{37}$$

For any pilot tones index set $\boldsymbol{q}_a$ that achieves Welch lower bound,

$$\psi_{\boldsymbol{q}_a}(d) = \frac{L-P}{(L-1)\,P}, \quad \forall d \in [1, \ldots, L-1], \qquad \lambda_{\boldsymbol{q}_a}(d) = 0, \quad \forall d \in [1, \ldots, L-1]. \tag{38}$$

By using the fact that $\sum_{v=1}^{N-1} n_v = P(P-1)$, $\lambda_{\boldsymbol{q}_a}(0)$ is given by

$$\lambda_{\boldsymbol{q}_a}(0) = \frac{P(P-1)}{L-1} + \sum_{v=1}^{N-1} n_v = \frac{PL(P-1)}{L-1}. \tag{39}$$

We can express $\{\lambda_{\boldsymbol{q}_a}(d)\}$ for $d \in [0, 1, \cdots, N-1]$ which satisfies (38) and (39) as

$$\lambda_{\boldsymbol{q}_a}(d) = \frac{PL(P-1)}{L-1}\sum_{l=0}^{L-1}\delta(d - lL). \tag{40}$$

Then, applying Fourier transform property, we obtain $\{n_v\}$ as

$$n_v = \frac{P(P-1)}{L-1}\sum_{k=0}^{L-1}\delta\left(v - k\frac{N}{L}\right). \tag{41}$$

Here n_v represents the frequency of cyclic difference value v of the pilot tones index set. So from definition 3, coherence of pilot tones index set $\{\boldsymbol{q}_a\}$ achieves Welch lower bound when $\{\boldsymbol{q}_a(\boldsymbol{u}, N, P, \Lambda)\}$ is GCDS with $\Lambda = \frac{P(P-1)}{L-1}$ and is a subset of $\left\{\boldsymbol{u} : u_m = \frac{N}{L}m; m = 0, 1, 2 \ldots (L-1)\right\}$. □

VII. ORTHOGONAL PILOTS FOR SPARSE CHANNELS

A. PROPOSED PILOT DESIGNS

Our orthogonal pilot design for sparse channels is based on the following criteria:

- Each pilot set should be orthogonal to all other pilot sets.
- CS based channel estimation performance should be similar for all the pilot sets to ensure fairness.
- Pilot sets should be optimized for CS based channel estimation performance.

Our design divides the full bandwidth into several pilot sets that are orthogonal in frequency. In section III, FDM type optimum orthogonal pilot design has been discussed for non-sparse channels. Cyclically equi-spaced pilots are optimum for non-sparse channel estimation when the total number of pilot tones P in a pilot set is equal to the number of channel tap L. In case of CS based sparse channel estimation where $P < L$, the channel estimation performance of equi-spaced pilot tones degrades. Proposition 2 shows that any cyclically equi-spaced pilot tones index set achieves maximum coherence when $P < L$. In other words, cyclically equi-spaced pilot tones have worst CS based channel estimation performance among all possible pilot sets. So here we propose two new orthogonal pilot designs (method A and B) suitable for CS based sparse channel estimation. We will use equal energy pilot tones for both of these methods. We also consider maximum channel length L to be a power of 2 for following pilot designs.

B. METHOD A

In method A, we design orthogonal pilot sets with similar and optimized channel estimation performances. Here we will use coherence as the CS based channel estimation performance metric. So our first design goal is to divide the set of all subcarriers into multiple orthogonal pilot sets with same coherence.

We achieve this goal in two steps using proposition 4 and proposition 5. According to proposition 4, coherence is not affected by the constant cyclical shift of the pilot tones. So in the first step we divide the set of all subcarriers into several orthogonal groups that are cyclically shifted versions of each others. This reduces the search space for optimized pilot sets considerably as we are able to choose an optimized pilot set from one of the subcarrier groups and use cyclically shifted version of that pilot set for all other groups. Pilot sets chosen in this way will have the same coherence. Proposition 5 states that the pilot sets that are mirror indexed pilot set (MIPS) of one another will have equal coherence. Thus, in the second step, we divide each of the subcarrier groups into two optimized pilot sets which are MIPS of one another. This ensures that all resulting orthogonal pilot sets will have the exact same coherence.

Now these steps bring us two design problems, namely how to design the subcarrier groups and how to divide each subcarrier group into two orthogonal pilot sets with optimized performances that are MIPS of one another. We first consider the problem of designing the subcarrier groups. As each orthogonal pilot set is chosen from the tones within one subcarrier group, their performance is limited by the tones spacings within that subcarrier group. According to proposition 2 and 3, the performance of a pilot set will be better than that of the cyclically equi-spaced pilot tones if it includes at least two adjacent pilot tones separated by N/L or less numbers of subcarriers. Another consideration is that for the maximum possible delay spread of L, the coherence bandwidth is N/L subcarriers. So pilot tones that are separated by less than N/L subcarriers will not contain more channel information than the pilot tones separated by N/L subcarriers. These design considerations lead to a logical grouping of cyclically equi-spaced tones that are separated by N/L subcarriers.

So we define the subcarrier groups by the orthogonal subcarrier index sets $\{J_i : i = 0, 1 \ldots D-1\}$ from section III where the total number of subcarrier groups $D = N/L$. $\{J_i\}$ contains cyclically equi-spaced tones indexes that are separated by N/L subcarriers with $J_i = \{(N/L)k + i : k = 0, 1, \ldots, (L-1)\}$.

The second design problem is how to divide each of the subcarrier groups with L tones into two optimized pilot sets that are MIPS of one another. For this problem, in method A we simply search through all possible MIPS pairs within the subcarrier group and choose the one with lowest coherence.

Let the MIPS pairs be defined by the pilot tones index sets $\{\boldsymbol{q}_i\}$ and $\{\boldsymbol{q}'_i\}$ for the group $\{J_i\}$. As the pilot sets are MIPS within $\{J_i\}$, we can set them as

$$\boldsymbol{q}'_i - i = (L-1)\frac{N}{L} - (\boldsymbol{q}_i - i) \tag{42}$$

where the specific shift of $(L-1)N/L$ is to accommodate the difference between $J_0[m]$ and $(N - J_0[L-1-m])$. From equation (42), $\{\boldsymbol{q}'_i\}$ can be expressed as

$$\boldsymbol{q}'_i = N - \boldsymbol{q}_i + \left(2i - \frac{N}{L}\right). \tag{43}$$

We can reduce the search space by using the relationship in equation (43). Let $\{J_{i,\alpha}\}$ and $\{J_{i,\beta}\}$ represent the $L/2$ subcarrier indexes respectively from first and second half of $\{J_i\}$. To find the MIPS pair, we first choose $k \in [0, 1, \ldots, L/4]$ tone indexes from the $\{J_{i,\alpha}\}$ and assign them to $\{\boldsymbol{q}_i\}$. Remaining tone indexes from $\{J_{i,\alpha}\}$ are assigned to $\{\boldsymbol{q}'_i\}$. Then we use equation (43) to assign the tones from $\{J_{i,\beta}\}$ to the pilot sets. So the size of our search space is now reduced to $\sum_{k=0}^{L/4}\binom{L/2}{k}$. This is much more tractable as it depends on the maximum channel length L instead of the DFT size N. Once we find the MIPS pair with minimum coherence for $\{J_i\}$, we can use cyclically shifted versions of the pilot sets for all other groups.

We now provide an example to illustrate the pilot design by method A. We use the example of DFT size $N = 128$,

the maximum channel length $L = 32$ and the number of non-zero channel taps equals to 5. First we divide all the subcarriers into $N/L = 4$ groups. Define the first subcarrier index group $\{J_0\} = [0, 4, \ldots, 124]$ containing 32 subcarrier indexes. Other groups are defined as $\{J_i\}$ where $J_i = J_0 + i$ and $i = 1, 2, 3$. Fig. 9 shows the four subcarrier groups.

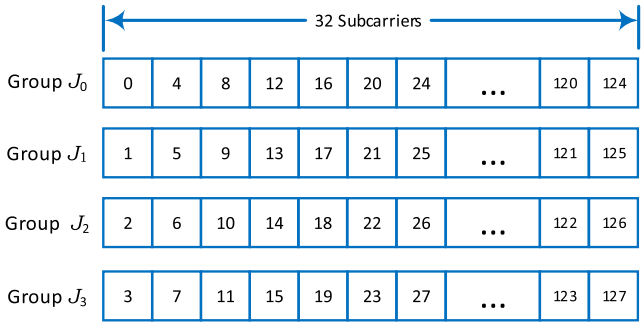

FIGURE 9. Subcarrier groups for $N = 128$, $L = 32$.

Next we divide $\{J_0\}$ into two pilot tones index sets $\{\boldsymbol{q}_0\}$ and $\{\boldsymbol{q}_0'\}$, each one containing $L/2 = 16$ pilot tones that are MIPS of each other. Fig. 10 shows the process of designing $\{\boldsymbol{q}_0\}$ and $\{\boldsymbol{q}_0'\}$. First we define subgroups $\{J_{0,\alpha}\} = [0, 4, \ldots, 60]$ and $\{J_{0,\beta}\} = [64, 68, \ldots, 124]$, which consist of the subcarrier indexes from the first and second half of $\{J_0\}$ respectively. We choose all possible k tones indexes from the subgroup $\{J_{0,\alpha}\}$ where $k \in [0, 1, \ldots, 8]$. There are a total of $\sum_{k=0}^{8} \binom{16}{k}$ possible combinations. Fig. 10 (a) shows a possible selection of $k = 7$ tones from $\{J_{0,\alpha}\}$. We assign the chosen k subcarrier indexes to $\{\boldsymbol{q}_0\}$ and the remaining indexes from $\{J_{0,\alpha}\}$ to $\{\boldsymbol{q}_0'\}$ as shown in Fig. 10 (b). Then we find the pilot indexes $\{128 - \boldsymbol{q}_0 - 4\}$ from $\{J_{0,\beta}\}$ and add them to $\{\boldsymbol{q}_0'\}$. Fig. 10 (c) shows this step. The remaining tone indexes from $\{J_{0,\beta}\}$ is added to $\{\boldsymbol{q}_0\}$. This completes the pilot tones index sets $\{\boldsymbol{q}_0\}$ and $\{\boldsymbol{q}_0'\}$ which is shown in Fig. 10 (d).

We calculate the coherence for all possible combinations of $\{\boldsymbol{q}_0\}$ and choose the one with lowest coherence. In this example $\{\boldsymbol{q}_0\}$ with minimum coherence is [0, 4, 12, 16, 40, 48, 60, 68, 72, 80, 88, 92, 96, 100, 104, 116]. Fig. 11 shows the $\{\boldsymbol{q}_0\}$ and $\{\boldsymbol{q}_0'\}$ associated with the lowest coherence.

We can find other six pilot tones index sets by using the relationship $\{\boldsymbol{q}_i\} = \{\boldsymbol{q}_0\} + i$ and $\{\boldsymbol{q}_i'\} = \{\boldsymbol{q}_0'\} + i$ where $i = 1, 2, 3$. For example $\{\boldsymbol{q}_1\} = [1, 5, 13, 17, 41, 49, 61, 69, 73, 81, 89, 93, 97, 101, 105, 117]$.

The steps for orthogonal pilot design using method A are summarized below.

1) Define the groups $\{J_i : i = 0, 1 \ldots D - 1\}$ containing L subcarrier indexes where $J_i = \{(N/L)k + i : k = 0, 1, \ldots, (L-1)\}$ and $D = N/L$.
2) Divide $\{J_0\}$ into two subgroups $J_{0,\alpha} = \{(N/L)k + i : k = 0, 1, \ldots, (L/2-1)\}$ and $J_{0,\beta} = \{(N/L)k + i : k = L/2, \ldots, (L-1)\}$.
3) Select all possible combinations of k tones from the subgroup $\{J_{0,\alpha}\}$ where $k \in [0, 1 \ldots, (L/4)]$. There are a total of $\sum_{k=0}^{L/4} \binom{L/2}{k}$ possible combinations.
4) For each combination of tones from the previous step, we will create two pilot tones index sets $\{\boldsymbol{q}_0\}$ and $\{\boldsymbol{q}_0'\}$ that are MIPS of each other. For each combination, assign the selected k tones to $\{\boldsymbol{q}_0\}$. Also assign the remaining unselected $(L/2 - k)$ tones from $\{J_{0,\alpha}\}$ to the pilot index set $\{\boldsymbol{q}_0'\}$.
5) Now for each combination, select k tones given by $\{N - \boldsymbol{q}_0 - N/L\}$ from subgroup $\{J_{0,\beta}\}$ and add them to set $\{\boldsymbol{q}_0'\}$. Add remaining unselected $(L/2 - k)$ tones from $\{J_{0,\beta}\}$ to set $\{\boldsymbol{q}_0\}$. This completes the pilot index sets $\{\boldsymbol{q}_0\}$ and $\{\boldsymbol{q}_0'\}$ with each one containing $L/2$ pilot tones.
6) For each combination, calculate the coherence of $\{\boldsymbol{q}_0\}$ and select the pilot tones index set with lowest coherence. Select $\{\boldsymbol{q}_0'\}$ that corresponds to the $\{\boldsymbol{q}_0\}$ with lowest coherence.
7) Select other pilot tones index sets as $\{\boldsymbol{q}_0 + i\}$ and $\{\boldsymbol{q}_0' + i\}$ where $i \in [1, \ldots, D-1]$.

C. METHOD B

Similar to method A, our first goal is to divide the full spectrum of N subcarriers into multiple orthogonal pilot sets with equal coherences. We use the same technique as in method A to divide the full spectrum into $D = N/L$ groups first. The groups are given by subcarrier index sets $\{J_i : i = 0, 1 \ldots D - 1\}$ where $J_i = \{(N/L)k + i : k = 0, 1, \ldots, (L-1)\}$. Next, we divide the group $\{J_i\}$ into two orthogonal pilot sets so that they are MIPS of each other. We start by constructing the MIPS pair for $\{J_0\}$ first.

While in method A we searched through all possible MIPS pairs to find the one with lowest coherence, the search space could become prohibitive when the maximum channel length L is large. We take a different approach in method B to construct an optimized MIPS pair that does not depend on an exhaustive search.

To design an optimized MIPS pair, we try to approximate some characteristics of the pilot set that achieves Welch lower bound. According to proposition 6, the pilot tones index set that achieves Welch lower bound is GCDS with all the pilot tones indexes taken from the group $\{J_0\}$. By definition within a GCDS all the distinct values of cyclic delays include all nonzero values of the members of $\{J_0\}$ and they will occur in exact same frequency. This frequency is given by $\Lambda = \frac{P(P-1)}{L-1}$ where P is the total number of pilots. We try to approximate this condition in our design. So our design goal is to construct the MIPS pair where within each pilot set all the distinct values for cyclic delays will occur with a frequency that is equal or close to Λ.

We try to accomplish this design goal in multiple steps. In each step we use two criteria to reduce the complexity of the design problem. First, in each step we try to achieve the frequency Λ for only one distinct value of the cyclic delays. We do this by selecting necessary pilot tones indexes in a specific pattern for each steps. We start with the smallest cyclic delay possible in the first step and use larger delays in an increasing order for successive steps. Second, instead of

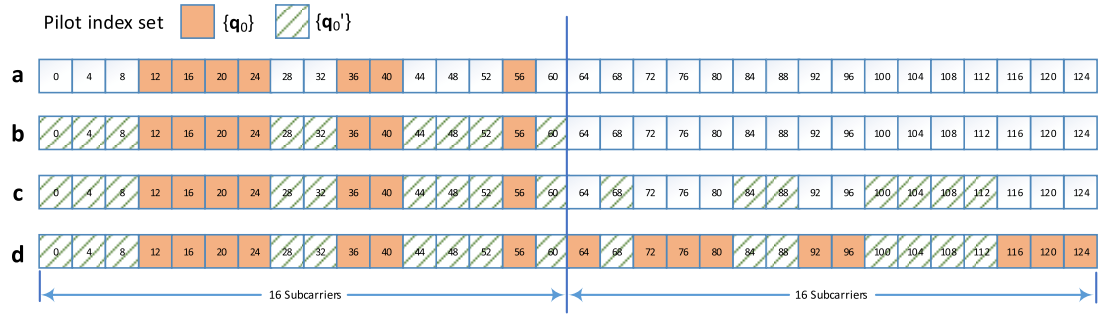

FIGURE 10. Steps for choosing mirror indexed pilot sets.

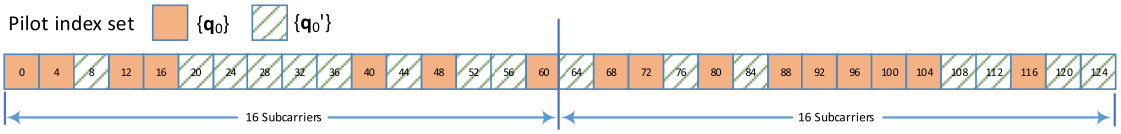

FIGURE 11. Orthogonal pilot sets using method A.

choosing pilot tones indexes from the full set of $\{J_0\}$, we first divide $\{J_0\}$ into smaller subgroups of equal sizes containing adjacent members of $\{J_0\}$. Then in each step we choose pilot tones indexes in a single pattern from one or more unused subgroups. We stop our design process when all the subgroups are assigned with a pilot tones pattern.

When designing the pilot sets using these steps, we face the design choices of how to define the subgroups, how many subgroups should we choose the pilot tones from in each step and what pattern should we use to choose those pilot tones.

Before further discussing these choices, we will first define all possible nonzero values of the members of $\{J_0\}$ as $\{v_k = (N/L)(k+1) : k = 0, \ldots, L-2\}$. So $\{v_k\}$ represents all possible distinct values for the cyclic differences for our design. In the r-th step we try to achieve the frequency Λ for cyclic differences of the value $v_r = (N/L)(r+1)$. Also we define the subgroup as a set of adjacent subcarrier indexes from $\{J_0\}$. We have limited choices for the size of each subgroup as we want to divide $\{J_0\}$ into equal sized subgroups. There are L subcarrier indexes in $\{J_0\}$ and L is a power of 2 in our design. So we limit the possible lengths of each subgroup to a power of 2.

While designing the subgroups, we use the following design considerations. First, using a larger subgroup size minimizes the number of steps necessary to design the pilot sets. Second, we also want to limit the size of subgroups so that in the r-th step the frequency of cyclic differences with value v_r does not exceed Λ. In each step we choose the pilot tones from at least one subgroup with a specific pattern. From a subgroup of size M, we can choose the most number of pilot tones when we use the pattern of $\{1, 1, \ldots, 1, 1\}$ of size M. Here $'1'$ in the pattern indicates that the corresponding subcarrier index is chosen for the pilot set. For such a pattern when applied to a subgroup, there will be a total of M cyclic differences within the selected pattern that are equal to v_0. So we design our subgroup size for this maximum case as $M = 2^{\lfloor \log_2 \Lambda \rfloor}$ which ensures that M is less than Λ and a power of 2.

In our design we divide $\{J_0\}$ into two orthogonal pilot tones index sets that are MIPS of each other. Let pilot tones index sets $\{\boldsymbol{q}_0\}$ and $\{\boldsymbol{q}'_0\}$ represent the MIPS pair. Because of the relationship between the MIPS pair in equation (43), each pilot tones pattern that is used for a subgroup in the first half of $\{J_0\}$ will have a corresponding pattern used for a subgroup in the second half of $\{J_0\}$. Let $\{\boldsymbol{s}_k\}$ and $\{\boldsymbol{s}'_k\}$ be the corresponding subgroups from the first and the second half of the $\{J_0\}$ where $k \in [0, 1, \ldots, R-1]$. The total number of subgroups is $2R = L/M$.

We define subgroup $\boldsymbol{s}_0 = \{(N/L)t : t = 0, 1 \ldots, M-1\}$ as the set of first M subcarrier indexes in $\{J_0\}$. Other groups are created by sequentially taking subcarrier indexes from $\{J_0\}$ and given by $\boldsymbol{s}_k = \boldsymbol{s}_0 + (N/L)Mk$. Relationship between $\{\boldsymbol{s}_k\}$ and $\{\boldsymbol{s}'_k\}$ is given by,

$$\boldsymbol{s}'_k = (L-1)\frac{N}{L} - \boldsymbol{s}_k. \tag{44}$$

Next we discuss the possible pilot tones index patterns. Let $\{\Gamma(v_r)\}$ represent the pilot tones index pattern used in the r-th step to select pilot tones from subgroup $\boldsymbol{s}_k$ and associated with cyclic difference v_r. For example, $\Gamma(v_0) = \{1, 1, \ldots, 1, 1\}$ selects pilot tones indexes from $\{\boldsymbol{s}_0\}$ in the first step. In the pattern $'1'$ indicates the selection of the corresponding subcarrier index for $\{\boldsymbol{q}_i\}$ while $'0'$ indicates a selection for $\{\boldsymbol{q}'_i\}$. Also let $\{\Gamma(v_r)'\}$ represent the corresponding pilot tones index pattern to select pilot tones from $\boldsymbol{s}'_k$. For the first step we use $\Gamma(v_0)' = \{0, 0, \ldots, 0, 0\}$ to select pilot tones from $\{\boldsymbol{s}'_0\}$. The pattern length should be the same as the subgroup length when possible. For larger values of v_i, the pattern length could be a multiple of subgroup length.

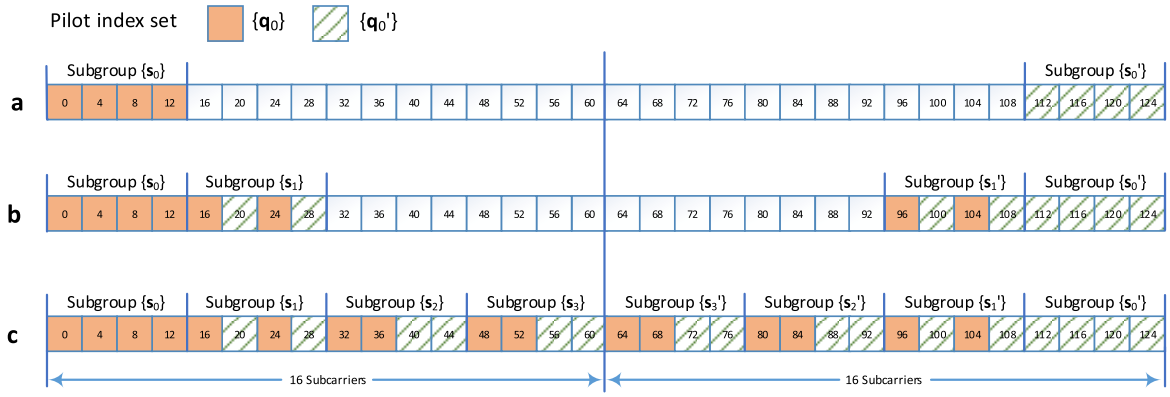

FIGURE 12. Orthogonal pilot sets using Method B.

While selecting the pattern for step r, we consider two criteria. First we want to minimize the number of cyclic differences within the pattern with a value less than v_r as they have already been considered in the previous steps. Second we want to maximize the number of cyclic difference value v_r. For example, using these criteria $\{1, 0, \ldots, 1, 0\}$ and $\{0, 1, \ldots, 0, 1\}$ both are possible pilot tones pattern for $\Gamma(v_1)$ that could be used in step 1 corresponding to v_1.

Finally, we consider the design problem of choosing the number of subgroups to be used in each step. For the first step we always choose the pilot tones from two subgroups $\{\boldsymbol{s}_0\}$ and $\{\boldsymbol{s}'_0\}$ using pattern $\Gamma(v_0)$ and $\Gamma(v_0)'$. Now let all the subgroups $\{\boldsymbol{s}_0\}, \ldots, \{\boldsymbol{s}_{k-1}\}$ and corresponding $\{\boldsymbol{s}'_0\}, \ldots, \{\boldsymbol{s}'_{k-1}\}$ be chosen in steps $0, \ldots, r-1$. For step r, we choose the pilots from the next available subgroups sequentially while the total number of cyclic differences of the value v_r within the chosen pilot tones does not exceed Λ. We start by choosing $\{\boldsymbol{s}_k\}$ and $\{\boldsymbol{s}'_k\}$. Next we choose $\{\boldsymbol{s}_{k+1}\}$ and $\{\boldsymbol{s}'_{k+1}\}$. We continue while there are subgroups available and the condition is not met. The pilot sets are complete when all the subgroups are chosen.

For other subcarrier groups we select pilot tones index sets as $\{\boldsymbol{q}_0 + i\}$ and $\{\boldsymbol{q}'_0 + i\}$ where $i \in [1, \ldots, N/L - 1]$.

We now give an example to illustrate our pilot design process using method B. We use the same example as in method A with DFT size $N = 128$, the maximum channel length $L = 32$ and 5 non-zero channel taps. Similar to method A, we divide the full bandwidth into 4 groups $\{J_i\}$ where $i = 0, 1, 2, 3$. The groups are shown in fig. 9. Next we divide the group $\{J_0\}$ into two pilot tones index sets $\{\boldsymbol{q}_0\}$ and $\{\boldsymbol{q}'_0\}$ with $P = 16$ pilots tones in each set.

For our example, $\Lambda = \frac{P(P-1)}{L-1} = 7.7419$. So we choose the size of subgroups $M = 2^{\lfloor log_2 \Lambda \rfloor} = 4$. Also define all possible cyclic differences within the pilot set as $\{\boldsymbol{v}\} = [4, 8, \ldots, 124]$.

In the first step, we assign the pattern $\{\Gamma(v_0)\} = \{1, 1, 1, 1\}$ to $\{\boldsymbol{s}_0\}$ and $\{\Gamma(v_0)'\} = \{0, 0, 0, 0\}$ to $\{\boldsymbol{s}'_0\}$. These patterns correspond to the cyclic differences of the value $v_0 = 4$. Fig. 12(a) shows this assignment.

In second step, we define the patterns $\{\Gamma(v_1)\} = \{\Gamma(v_1)'\} = \{1, 0, 1, 0\}$ associated with $v_1 = 8$. We first assign this pattern to subgroups $\{\boldsymbol{s}_1\}$ and $\{\boldsymbol{s}'_1\}$. After this assignment, there are a total of 5 cyclic differences that are equal to v_1 within the assigned pilot tones. As this value is less than Λ, we continue with the same pattern. When we assign these patterns to next available subgroups $\{\boldsymbol{s}_2\}$ and $\{\boldsymbol{s}'_2\}$, the total number of cyclic differences that are equal to v_1 exceeds Λ and hence this step is not performed. So we go to next step after assigning the first set of subgroups. Fig. 12(b) shows this step.

In the third step, we define the patterns $\{\Gamma(v_2)\} = \{\Gamma(v_2)'\} = \{1, 1, 0, 0, 1, 1, 0, 0\}$ and choose pilot tones from the subgroups $\{\boldsymbol{s}_2\}$, $\{\boldsymbol{s}_3\}$ and $\{\boldsymbol{s}'_2\}$, $\{\boldsymbol{s}'_3\}$ using this pattern. Fig. 12(c) shows the final assignment.

The steps to design orthogonal pilot sets using method B are summarized as follows.

1) Define the groups $\{J_i : i = 0, 1 \ldots D-1\}$ containing L subcarrier indexes where $J_i = \{(N/L)k + i : k = 0, 1, \ldots, (L-1)\}$ and $D = N/L$.
2) Find $\Lambda = \frac{P(P-1)}{L-1}$.
3) Define the subgroup size $M = 2^{\lfloor \log_2 \Lambda \rfloor}$.
4) Define the subgroups $\boldsymbol{s}_k = \{(N/L)(t + Mk) : t = 0, 1 \ldots, M-1\}$ and $k = [0, 1, \ldots, (L/2M) - 1]$ by sequentially using M subcarrier indexes from the first half of $\{J_0\}$ for each subgroup. Also define the corresponding subgroups from the second half of $\{J_0\}$ as $\boldsymbol{s}'_k = (L-1)\frac{N}{L} - (\boldsymbol{s}_k)$.
5) In the first step assign the pilot tones index pattern $\{\Gamma(v_0)\} = \{1, \ldots, 1\}$ to $\{\boldsymbol{s}_0\}$ and $\{\Gamma(v_0)'\} = \{0, \ldots, 0\}$ to $\{\boldsymbol{s}'_0\}$.
6) In the r-th step define the pilot tones index pattern $\{\Gamma(v_r)\}$ and $\{\Gamma(v_r)'\}$ using the criteria described previously. Continue assigning these patterns to next available subgroup sets while the total number of cyclic differences that are equal to v_2 within the set of selected pilot tones does not exceed Λ.
7) Stop the assignment process when all the subgroups have been selected. Assign all subcarrier indexes corresponding to '1' to $\{\boldsymbol{q}_0\}$ and all others to $\{\boldsymbol{q}'_0\}$.
8) Select other pilot tones index sets as $\{\boldsymbol{q}_0 + i\}$ and $\{\boldsymbol{q}'_0 + i\}$ where $i \in [1, \ldots, N/L - 1]$.

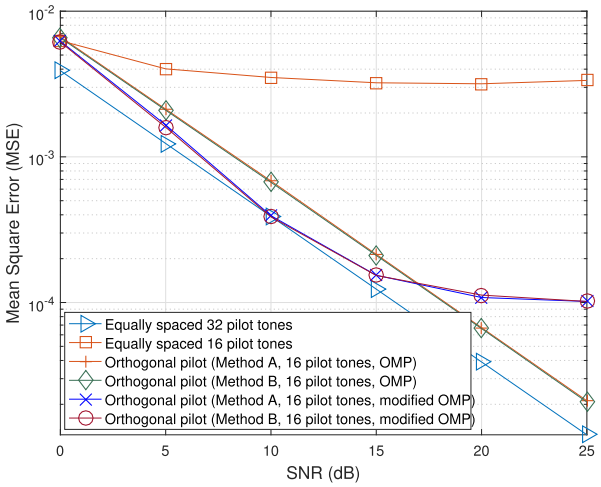

FIGURE 13. Channel estimation performance comparison for different orthogonal pilot designs with $N = 128$ subcarriers, $L = 32$ channel length and 5 non-zero channel taps.

D. CHANNEL ESTIMATION PERFORMANCE

Fig. 13 shows the performances of different orthogonal pilot designs for CS and that of optimum pilot set with equally spaced 32 non-zero pilots. For the simulation, we have used the same example that we have used for method A and B. The sparse channel is modeled according to section II with 5 non-zero channel taps. The performance results are averaged over 10000 simulation trials. The positions of non-zero channel taps are generated randomly for each trial. OMP algorithm in Appendix is used for CS based channel estimation. To limit the contribution of noise for low to medium SNR scenario (thus improving the channel estimation performance), we have also implemented a modified OMP algorithm. For the modification, we have added an extra step after the original OMP algorithm where we select only the non-zero channel taps which are within -20dB of the strongest channel tap. From Fig. 13, the channel estimation performances for method A and method B are similar. Their performances are considerably better than the equally spaced 16 pilot tones. We also observe that the modified OMP algorithm performs better for medium to low SNR compared to the original OMP algorithm. At higher SNR where the noise contribution is low, we see a performance floor for the modified OMP algorithm due to the removal of smaller channel taps.

VIII. NON-ORTHOGONAL PILOTS FOR SPARSE CHANNEL

A. PROPOSED PILOT DESIGN

The strategy for CS based non-orthogonal pilot design is similar to the one used for non-sparse channel. For non-orthogonal pilot design we use our orthogonal pilot design in method B as a baseline. We set some of the pilot tones from the original pilot sets as null. Different combinations of null tones provide different non-orthogonal pilot sequences. We apply following design considerations to define the possible locations of null pilots. For an orthogonal pilot set with P pilot tones, let the non-orthogonal pilot sequences have $P' < P$ non-zero pilot tones and $P'' = P - P'$ null pilot tones. From proposition 6, the pilot sequence that achieves Welch lower bound with P' non zero pilot tones will have each one of all distinct cyclic differences exactly $\Lambda(P') = \frac{P'(P'-1)}{L-1}$ times. Now $\Lambda(P') < \Lambda(P)$ as $P' < P$. This indicates that we should spread the null pilot tones within all the pilot tones patterns so that it decreases the total number of cyclic differences that are equal to v_i by the same amount for all $i = 1, 2, \ldots, L-1$. While we cannot achieve this condition exactly, we approximate this condition by using one null pilot tones within each of the subgroup pairs $\{\boldsymbol{s}_i\}$ and $\{\boldsymbol{s}'_i\}$, $i = 0, 1, \ldots, R$, as defined in section VII-C.

Let there be a total of P_s pilot tones indexes within the subgroup pair $\{\boldsymbol{s}_i\}$ and $\{\boldsymbol{s}'_i\}$. We use one of these P_s pilot tones as null for non-orthogonal pilot sequences. For a total of R null tones, one for each subgroup pairs, there could be a total of P_s^R non-orthogonal sequences possible from one orthogonal pilot set. Following are the steps to design non-orthogonal pilot sequences for the sparse channel.

1) Follow the steps in section VII-C and design orthogonal pilot set using method B for CS based sparse channel estimation.
2) Choose an orthogonal pilot index set as a baseline. We choose $\{\boldsymbol{q}_0\}$ as the first set.
3) Use one pilot tone as null pilot from each one of the subgroup pairs $\{\boldsymbol{s}_i\}$ and $\{\boldsymbol{s}'_i\}$, $i = 0, 1, \ldots, R-1$.
4) Selected R null pilot tones and $P - R$ non-zero pilot tones create a non-orthogonal pilot sequence.
5) Each combination of null pilot tones will create one non-orthogonal pilot sequence. There are P_s^R non-orthogonal pilot sequences when P_s is the number of pilot tones in each subgroup pair.
6) Similarly generate non-orthogonal pilot sequences for $\{\boldsymbol{q}'_0\}$ and other orthogonal pilot sets. For $2N/L$ orthogonal pilot sets in our design, there will be a total of $2P_s^R N/L$ non-orthogonal pilot sequences possible using the whole bandwidth.

We use the same example from section VII-C with DFT size $N = 128$ and the maximum channel length $L = 32$ to illustrate our non-orthogonal pilot design. There are a total of $2N/L = 8$ orthogonal pilot sets. Fig. 12(c) shows the orthogonal pilot tones index set $\{\boldsymbol{q}_0\}$ and $\{\boldsymbol{q}'_0\}$. There are $R = 4$ subgroup pairs $\{\boldsymbol{s}_i\}$ and $\{\boldsymbol{s}'_i\}$, $i = 0, 1, 2, 3$ containing $\{\boldsymbol{q}_0\}$ and $\{\boldsymbol{q}'_0\}$. Each subgroup pair has $P_s = 4$ pilot tone indexes that are included in $\{\boldsymbol{q}_0\}$. We choose one of these 4 pilot tones from each subgroup pairs as a null pilot tone. Each combination of null pilot tones generates a non-orthogonal pilot sequence. Fig. 14 shows an example of non-orthogonal pilot sequence from orthogonal pilot set $\{\boldsymbol{q}_0\}$. In this example the null pilot tone indexes are {8, 36, 68, 104}. Using different combinations of null pilot tones creates a total of $2P_s^R N/L = 2048$ non-orthogonal pilot sequences.

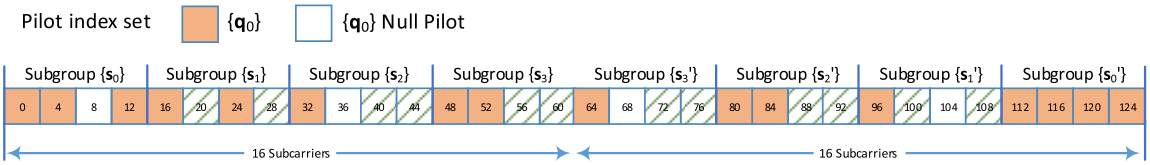

FIGURE 14. Non-orthogonal pilot sequence with 12 non-zero pilots and 4 null pilots.

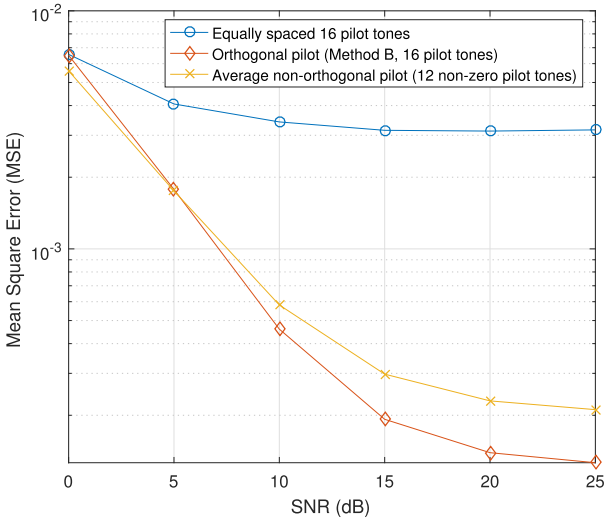

FIGURE 15. Channel estimation performance comparison for orthogonal and non-orthogonal pilot designs with $N = 128$ subcarriers, $L = 32$ channel length and 5 non-zero channel taps.

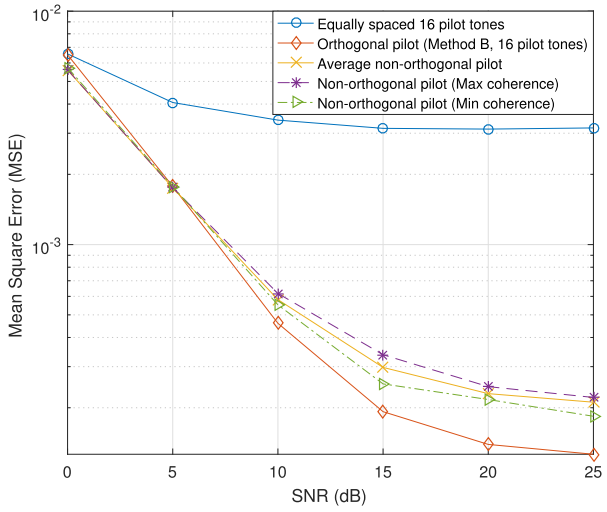

FIGURE 16. Best and worst channel estimation performances of non-orthogonal pilot sequences with $N = 128$ subcarriers, $L = 32$ channel length and 5 non-zero channel taps.

B. CHANNEL ESTIMATION PERFORMANCE

Fig. 15 shows the average channel estimation performance of non-orthogonal pilot sequences compared with that of orthogonal pilot sequences. For simulation we have used the same example that has been used in section VII and VIII. While the average performances for non-orthogonal pilot sequences are lower than orthogonal pilot codes due to the use of less non-zero pilot tones, the performance is considerably better than that of equally spaced pilots tones. Fig. 16 shows the performances for non-orthogonal pilot sequences with the best and the worst coherence. These results show comparable performance for all non-orthogonal pilot sequences, thus providing fairness among users.

IX. CONCLUSIONS

In this paper, first we have developed a novel non-orthogonal pilot design for non-sparse channel that outperforms the existing design in channel estimation performance, supports collision detection at the receiver and could accommodate a large number of users through non-orthogonal pilot codes. Also we have developed an optimum threshold based pilot detection scheme. Our simulation results show that when the detection threshold is dynamically set, it could lead to better performance over a broader SNR range. We have also presented two non-orthogonal pilot designs for systems using a fractional bandwidth allocation. Both of these schemes provide similar or better channel estimation performances compared to the existing design while supporting a higher number of non-orthogonal users and providing collision detection capability. For CS based sparse channel estimation we have proposed two orthogonal pilot designs. Then we have further developed non-orthogonal pilot designs with collision detection capabilities for CS based channel estimation. Simulation results corroborate that our designs provide fairness and optimized channel estimation performance among users.

APPENDIX

Here we provide OMP algorithm used for CS based channel estimation [11]. To describe the algorithm, we use the system description from equation (14) where the received frequency domain pilot vector is given by

$$\boldsymbol{Y}_P = \boldsymbol{A}(\boldsymbol{q})\boldsymbol{h} + \boldsymbol{n}. \tag{45}$$

Here $\boldsymbol{A}(\boldsymbol{q}) = [A_0, A_1, \ldots, A_{L-1}]$ is the dictionary matrix and A_i is the i-th column of the dictionary matrix. The OMP algorithm is as follows.

1) **Initialize** the residual $\boldsymbol{R}_0 = \boldsymbol{Y}_P$, the set of selected indexes for non-zero components $\{\boldsymbol{S}\} = \emptyset$ and the iteration counter $i = 1$.

2) **Find** the index $d_i = k$ that solves $\max_k \left|A_k' \boldsymbol{R}_{i-1}\right|$.
3) **Update** the set $\{\boldsymbol{S}\} = \{\boldsymbol{S}\} \cup d_i$.
4) **Define** the set $\boldsymbol{A}(\boldsymbol{S})$ as the submatrix of $\boldsymbol{A}(\boldsymbol{q})$ being comprised of the columns with indexes from set $\{\boldsymbol{S}\}$.
5) **Find** the projection $\boldsymbol{B}_i = \boldsymbol{A}(\boldsymbol{S})\left(\boldsymbol{A}(\boldsymbol{S})'\boldsymbol{A}(\boldsymbol{S})\right)^{-1}\boldsymbol{A}(\boldsymbol{S})'$.
6) **Update** the residual $\boldsymbol{R}_i = (\boldsymbol{I} - \boldsymbol{B}_i)$ and the iteration counter $i = i + 1$.
7) **Go to** step 9 if $||\boldsymbol{R}_i||^2 \leq \sigma_n^2$.
8) **Return** to step 2.
9) **Calculate** the estimate, $\hat{\boldsymbol{h}} = \left(\boldsymbol{A}(\boldsymbol{S})'\boldsymbol{A}(\boldsymbol{S})\right)^{-1}\boldsymbol{A}(\boldsymbol{S})'\boldsymbol{Y}_P$

REFERENCES

[1] C. Bockelmann *et al.*, "Massive machine-type communications in 5G: Physical and MAC-layer solutions," *IEEE Commun. Mag.*, vol. 54, no. 9, pp. 59–65, Sep. 2016.
[2] M. Peng, S. Yan, and H. V. Poor, "Ergodic capacity analysis of remote radio head associations in cloud radio access networks," *IEEE Wireless Commun. Lett.*, vol. 3, no. 4, pp. 365–368, Aug. 2014.
[3] H. Ishii, Y. Kishiyama, and H. Takahashi, "A novel architecture for LTE-B: C-plane/U-plane split and phantom cell concept," in *Proc. Globecom Workshops (GC Wkshps)*, Dec. 2012, pp. 624–630.
[4] S. Chen, F. Qin, B. Hu, X. Li, and Z. Chen, "User-centric ultra-dense networks for 5G: Challenges, methodologies, and directions," *IEEE Wireless Commun.*, vol. 23, no. 2, pp. 78–85, Apr. 2016.
[5] J. Zhang *et al.*, "PoC of SCMA-based uplink grant-free transmission in UCNC for 5G," *IEEE J. Sel. Areas Commun.*, vol. 35, no. 6, pp. 1353–1362, Jun. 2017.
[6] T. L. Marzetta, "Noncooperative cellular wireless with unlimited numbers of base station antennas," *IEEE Trans. Wireless Commun.*, vol. 9, no. 11, pp. 3590–3600, Nov. 2010.
[7] O. Y. Bursalioglu, C. Wang, H. Papadopoulos, and G. Caire, "RRH based massive MIMO with 'on the Fly' pilot contamination control," in *Proc. IEEE Int. Conf. Commun. (ICC)*, May 2016, pp. 1–7.
[8] O. Y. Bursalioglu, C. Wang, H. Papadopoulos, and G. Caire, "A novel alternative to cloud RAN for throughput densification: Coded pilots and fast user-packet scheduling at remote radio heads," in *Proc. 15th Asilomar Conf. Signals, Syst. Comput.*, Nov. 2016, pp. 3–10.
[9] Z. Li, N. Rupasinghe, O. Y. Bursalioglu, C. Wang, H. Papadopoulos, and G. Caire, "Directional training and fast sector-based processing schemes for mmWave channels," in *Proc. IEEE Int. Conf. Commun. (ICC)*, May 2017, pp. 1–7.
[10] W. U. Bajwa, J. Haupt, A. M. Sayeed, and R. Nowak, "Compressed channel sensing: A new approach to estimating sparse multipath channels," *Proc. IEEE*, vol. 98, no. 6, pp. 1058–1076, Jun. 2010.
[11] T. T. Cai and L. Wang, "Orthogonal matching pursuit for sparse signal recovery with noise," *IEEE Trans. Inf. Theory*, vol. 57, no. 7, pp. 4680–4688, Jul. 2011.
[12] W. Dai and O. Milenkovic, "Subspace pursuit for compressive sensing signal reconstruction," *IEEE Trans. Inf. Theory*, vol. 55, no. 5, pp. 2230–2249, May 2009.
[13] E. Candes and T. Tao, "The Dantzig selector: Statistical estimation when p is much larger than n," *Ann. Statist.*, vol. 35, no. 6, pp. 2313–2351, 2007.
[14] W. C. Ao, C. Wang, O. Y. Bursalioglu, and H. Papadopoulos, "Compressed sensing-based pilot assignment and reuse for mobile UEs in mmWave cellular systems," in *Proc. IEEE Int. Conf. Commun. (ICC)*, May 2016, pp. 1–7.
[15] Y. Li, H. Minn, N. Al-Dhahir, and A. R. Calderbank, "Pilot designs for consistent frequency-offset estimation in OFDM systems," *IEEE Trans. Commun.*, vol. 55, no. 5, pp. 864–877, May 2007.
[16] L. S. Louis, *Statistical Signal Processing: Detection, Estimation, and Time Series Analysis*. Reading, MA, USA: Addison-Wesley, 1991.
[17] H. Minn and N. Al-Dhahir, "Optimal training signals for MIMO OFDM channel estimation," *IEEE Trans. Wireless Commun.*, vol. 5, no. 5, pp. 1158–1168, May 2006.
[18] E. J. Candès and M. B. Wakin, "An introduction to compressive sampling," *IEEE Signal Process. Mag.*, vol. 25, no. 2, pp. 21–30, Mar. 2008.
[19] D. L. Donoho, M. Elad, and V. N. Temlyakov, "Stable recovery of sparse overcomplete representations in the presence of noise," *IEEE Trans. Inf. Theory*, vol. 52, no. 1, pp. 6–18, Jan. 2006.
[20] L. Welch, "Lower bounds on the maximum cross correlation of signals (Corresp.)," *IEEE Trans. Inf. Theory*, vol. 20, no. 3, pp. 397–399, May 1974.
[21] P. Xia, S. Zhou, and G. B. Giannakis, "Achieving the Welch bound with difference sets," *IEEE Trans. Inf. Theory*, vol. 51, no. 5, pp. 1900–1907, May 2005.

AYON QUAYUM (S'17) received the B.Sc. degree in electrical and electronic engineering from the Bangladesh University of Engineering and Technology, Dhaka, Bangladesh, in 2005, the M.Sc. degree in electrical and computer engineering from North Carolina State University, NC, USA, in 2008. He is currently pursuing the Ph.D. degree in electrical engineering with The University of Texas at Dallas, Richardson, TX, USA. From 2008 to 2016, he was a Staff Engineer in Qualcomm Inc., where he was involved in research and development of WCDMA and 4G systems. His research interests include signal processing, wireless communication, and system design for next-generation wireless standards.

HLAING MINN (S'99–M'01–SM'07–F'16) received the B.E. degree in electrical and electronic engineering from the Yangon Institute of Technology, Yangon, Myanmar, in 1995, the M.E. degree in telecommunications from the Asian Institute of Technology, Thailand, in 1997, and the Ph.D. degree in electrical engineering from the University of Victoria, Victoria, BC, Canada, in 2001. He was a Post-Doctoral Fellow with the University of Victoria in 2002. He has been with The University of Texas at Dallas, USA, since 2002, where he is currently a Full Professor. His research interests include wireless communications, signal processing, signal design, dynamic spectrum access and sharing, next generation wireless technologies, and bio-medical signal processing.

Dr. Minn has served as a technical program committee member for over 30 IEEE conferences. He has served as the Technical Program Co-Chair for the Wireless Communications Symposium of the IEEE GLOBECOM 2014 and the Wireless Access Track of the IEEE VTC, in 2009. He served as an Editor for the IEEE TRANSACTIONS ON COMMUNICATIONS from 2005 to 2016. He was also an Editor for the *International Journal of Communications and Networks* from 2008 to 2015. He has been serving as an Editor-at-Large for the IEEE TRANSACTIONS ON COMMUNICATIONS since 2016.

YUICHI KAKISHIMA received the B.S. and M.S. degrees from the Tokyo Institute of Technology, Tokyo, Japan, in 2005 and 2007, respectively. From 2015 to 2018, he was with DOCOMO Innovations, Inc., USA (a subsidiary of NTT DOCOMO) as a Manager for 5G and Beyond 5G Research and 3GPP Standardization. He is currently an Assistant Manager with NTT DOCOMO, INC., where he has been involved in the research and development of wireless access technologies, including multi-antenna techniques for 5G and LTE-Advanced systems. He is also involved in 3GPP standardization as a delegate of 3GPP RAN1 and RAN4.